


KCTD8 and KCTD12 Facilitate Axonal Expression of GABA_B Receptors in Habenula Cholinergic Neurons

Yuqi Ren,^{1*} Yang Liu,^{2,3,4*} Sanduo Zheng,^{1,5} and  Minmin Luo^{1,3,4,5}

¹National Institute of Biological Sciences, Beijing 102206, China, ²School of Life Sciences, Tsinghua University, Beijing 100084, China, ³Tsinghua-Peking Center for Life Sciences, 100084 Beijing, China, ⁴Chinese Institute for Brain Research, Beijing 102206, China, and ⁵Tsinghua Institute of Multidisciplinary Biomedical Research, Beijing 102206, China

GABA_B receptors in habenula cholinergic neurons mediate strong presynaptic excitation and control aversive memory expression. K⁺ channel tetramerization domain (KCTD) proteins are key interacting partners of GABA_B receptors; it remains unclear whether and how KCTDs contribute to GABA_B excitatory signaling. Here, we show that KCTD8 and KCTD12 in these neurons facilitate the GABA_B receptors expression in axonal terminals and contribute to presynaptic excitation by GABA_B receptors. Genetically knocking out *KCTD8/12/16* or *KCTD8/12*, but not other combinations of the three *KCTD* isoforms, substantially reduced GABA_B receptors-mediated potentiation of glutamate release and presynaptic Ca²⁺ entry in response to axonal stimulation, whereas they had no effect on GABA_B-mediated inhibition in the somata of cholinergic neurons within the habenulo–interpeduncular pathway in mice of either sex. The physiological phenotypes were associated with a significant decrease in the GABA_B expression within the axonal terminals but not the somata. Overexpressing either KCTD8 or KCTD12 in the *KCTD8/12/16* triple knock-out mice reversed the changes in axonal GABA_B expression and presynaptic excitation. In mice lacking the KCTDs, aversion-predicting cues produced stronger neuronal activation in the interpeduncular nucleus, and the infusion of GABA_B agonist in this nucleus produced a weaker effect on fear extinction. Collectively, our results reveal isoform-specific roles of KCTD proteins in enriching the axonal expression of GABA_B receptors, facilitating their presynaptic signaling, and modulating aversion-related memory processes.

Key words: baclofen; Ca²⁺ imaging; GABA_B auxiliary subunits; habenulo–interpeduncular pathway; K⁺ channel tetramerization domain; optogenetics

Significance Statement

GABA_B receptors represent the principal inhibitory neurotransmitter receptor, but they mediate strong presynaptic excitation in the habenulo–interpeduncular pathway and modulate aversion memory expression. KCTD proteins are integral constituents of GABA_B receptors. By analyzing the physiological, neuroanatomical, and behavioral phenotypes of multiple KCTD knock-out mouse lines, we show that KCTD8 and KCTD12 facilitate the axonal expression and hence presynaptic excitation of GABA_B receptors in habenula cholinergic neurons and control cued-aversion memory formation and expression in the habenulo–interpeduncular pathway. These results expand the physiological and behavioral functions of KCTDs in modulating the brain neural circuits.

Introduction

The cholinergic pathway projecting from the ventral part of the medial habenula (MHb) to the rostral and central core of the

interpeduncular nucleus (IPN) controls aversive memories, anxiety, fear responses, and nicotine dependence in vertebrates (Kim, 2009; Qin and Luo, 2009; Quina et al., 2009; Agetsuma et al., 2010; Frahm et al., 2011; Kobayashi et al., 2013; Yamaguchi et al., 2013; Frahm et al., 2015; Soria-Gómez et al., 2015; Ables et al., 2017; Zhang et al., 2017). Habenula cholinergic neurons corelease glutamate, acetylcholine, and neurokinin B to activate postsynaptic neurons in the IPN (Ren et al., 2011; Zhang et al., 2016). GABA_B receptors—heteromeric G-protein-coupled receptors composed of the GABA_{B1} and GABA_{B2} subunits—are highly expressed in these neurons (Gassmann and Bettler, 2012; Zhang et al., 2016; Fritzius and Bettler, 2020). Although GABA_B receptors are predominantly inhibitory in the brain (Gassmann and Bettler, 2012), they mediate strong presynaptic excitation in the

Received Aug. 17, 2021; revised Dec. 18, 2021; accepted Dec. 30, 2021.

Author contributions: M.L., Y.R., Y.L., and S.Z. designed research; Y.R. and Y.L. performed research; Y.R. and Y.L. analyzed data; and M.L., Y.R., and Y.L. wrote the paper.

This work was supported by the Beijing Municipal Government. We thank Bernhard Bettler (University of Basel) for the *KCTD8/12/16* KO mice, Bin Li (National Institute of Biological Sciences, Beijing) for advice on statistical tests, and J. H. Snyder and other Luo lab members for comments.

*Y.R. and Y.L. contributed equally to this work.

The authors declare no competing financial interests.

Correspondence should be addressed to Minmin Luo at luominmin@nibs.ac.cn.

<https://doi.org/10.1523/JNEUROSCI.1676-21.2021>

Copyright © 2022 the authors

habenulo–interpeduncular pathway by amplifying presynaptic Ca²⁺ entry through Ca_{v2.3} channels and potentiating neurotransmitter corelease to IPN neurons (Zhang et al., 2016). At the behavior level, inactivating GABA_B receptors in habenula cholinergic neurons impairs the extinction of aversive memory in mice (Zhang et al., 2016).

Cytosolic K⁺ channel tetramerization domain (KCTD) proteins KCTD8, 12, 12b, and 16 assemble with GABA_B receptors by interacting with the GABA_{B2} subunit (Schwenk et al., 2010, 2016). The different KCTDs are known to exert a variety of effects on GABA_B-mediated responses. For example, KCTD12, 12b, and 16 shorten the rise time of GABA_B-induced opening of potassium channels and facilitate the desensitization of GABA_B receptors in cultured cells (Schwenk et al., 2010; Seddik et al., 2012; Turecek et al., 2014; Fritzius et al., 2017; Zheng et al., 2019; Zuo et al., 2019). The GABA_B-associated KCTDs exhibit a distinct spatial and temporal distribution pattern in the mammalian brain and have been implicated in neuropsychiatric disorders in humans (Metz et al., 2011; Teng et al., 2019).

Several KCTDs are richly expressed in MHb neurons (Metz et al., 2011). Considering that GABA_B-mediated presynaptic excitation in habenula neurons and that KCTD proteins modulate the kinetics of GABA_B-mediated responses, we asked whether and how KCTDs affect GABA_B-mediated presynaptic excitation in the MHb–IPN pathway. Recently, Bhandari et al. (2021) showed that KCTD8 and KCTD12b modulate Ca_{v2.3}-mediated release from MHb terminals but are not involved in GABA_B receptors–mediated presynaptic excitation. This study did not examine the potential roles of KCTD12 and KCTD16. Here, we took advantage of the recently developed *KCTD8*, *12*, and *16* triple knock-out (3KO) mouse model (Rajalu et al., 2015) and various combinations of isoform deficiency to investigate the role of KCTDs on GABA_B signaling in habenula cholinergic neurons. Our results reveal that KCTDs have a strong contribution to GABA_B axonal expression and presynaptic excitation, but not soma expression and postsynaptic inhibition, with KCTD8 and KCTD12 playing important and redundant roles. Our data demonstrate isoform- and site-specific association of KCTDs with presynaptic GABA_B receptors expression and expand the physiological and behavioral functions of KCTDs in modulating the brain neural circuits.

Materials and Methods

Animals. All procedures were conducted following the approval of the Animal Care and Use Committee of the National Institute of Biological Sciences, Beijing, in accordance with the governmental regulations of China. We used adult mice (8–12 weeks, 18–25 g) of either sex for the patch-clamp recording, two-photon Ca²⁺ imaging, and immunostainings. We used adult male mice for the aversive conditioning, fiber photometry, and intra-IPN drug infusion. The *ChAT-ChR2-EYFP* BAC-transgenic mice were a gift from G. Feng (Massachusetts Institute of Technology) and had been crossed to the C57BL/6N background for more than 10 generations. Homozygous *KCTD8/12/16* KO mice were a gift from Bernhard Bettler (University of Basel). We crossed *ChAT-ChR2-EYFP* BAC-transgenic mice with *KCTD8/12/16* KO mice to obtain *ChAT-ChR2-EYFP* mice with heterozygous *KCTD8/12/16* as F1. By self-fertilizing the F1 generation, we obtained *ChAT-ChR2-EYFP* mice with different types of KCTD deficiency: *KCTD8* KO::*ChAT-ChR2*, *KCTD12* KO::*ChAT-ChR2*, *KCTD16* KO::*ChAT-ChR2*, *KCTD8/12* KO::*ChAT-ChR2*, and *KCTD8/12/16* KO::*ChAT-ChR2* mice. All mice were bred and maintained at a specific-pathogen-free mouse facility. Wild-type (WT) C57BL/6N mice were purchased from VitalRiver. All mice were maintained on controlled temperature (22–25°C) and a 12/12 light/dark cycle with access to food and water *ad libitum*.

AAV preparation and injection. Adeno-associated virus (AAV) vectors carrying *GCaMP6m*, *mCherry*, *KCTD8-P2A-mCherry*, and *KCTD12-P2A-mCherry* were packaged into 2/9 serotypes with titers of 1–5 × 10¹² viral particles/ml. We constructed the plasmid pAAV-EF1a-GCaMP6m by replacing the coding region of *DIO-ChR2-mCherry* in pAAV-EF1a-DIO-hChR2 (H134R)-mCherry plasmid (catalog #20297, Addgene; a gift from Dr. Karl Deisseroth) with that of *GCaMP6m* plasmid (catalog #40754, Addgene; a gift from Dr. Douglas Kim). The *KCTD8* and *KCTD12* sequences were cloned from mouse brain cDNA. We built a fusion construct that was composed of the sequences for KCTD, the P2A peptide, and an mCherry reporter (*KCTD-P2A-mCherry*). These fusion constructs were inserted into a pAAV-EF1a backbone.

For AAV injections, adult mice were anesthetized with pentobarbital (80 mg/kg, i.p.) and then mounted on a stereotaxic apparatus. The skin was cut, and a small craniotomy was performed above the MHb or the IPN. Injections were performed using a microsyringe pump (Nanoliter 2010 injector, World Precision Instruments). A micro controller (World Precision Instruments) was used to deliver the virus solution to the target areas at a rate of 46 nl/min. The following coordinates were used to target specific brain areas: 1.3–1.7 mm posterior to the bregma, 0.1 mm lateral to midline, and 2.6 mm ventral to the skull surface for the MHb; 3.4 mm posterior to the bregma, 1.25 mm lateral to midline, and 4.8 mm ventral to the skull surface with a 15° angle (lateral to midline) for the IPN.

Brain slice preparation, patch-clamp recording, and two-photon Ca²⁺ imaging. Adult mice were anesthetized with pentobarbital (80 mg/kg, i.p.) and then transcardially perfused with 5 ml ice-cold oxygenated slice solution (saturated with 95% O₂ and 5% CO₂). The slice solution contains the following as reagent (in mM): 110 choline chloride, 2.5 KCl, 0.5 CaCl₂, 7 MgCl₂, 1.3 NaH₂PO₄, 25 NaHCO₃, 10 glucose, 1.3 Na-ascorbate, and 0.6 Na-pyruvate. The slice solution was adjusted to 305–315 mOsm/L using sucrose. Next, the mouse brains were dissected and transferred into ice-cold oxygenated slice solution. Brains were first blocked at a 54° deviate angle from the horizontal plane, and sections containing the MHb–IPN pathway (200 μm, two per mouse) were cut with a vibratome (VT1200s, Leica). Slices were incubated for at least 1 h at 33°C within oxygenated artificial cerebrospinal fluid (ACSF) containing the following (in mM): 125 NaCl, 2.5 KCl, 2 CaCl₂, 1.3 MgCl₂, 1.3 NaH₂PO₄, 1.3 Na-ascorbate, 0.6 Na-pyruvate, 10 glucose, and 25 NaHCO₃ (305–315 mOsm/L). The brain slices were transferred to a recording chamber at room temperature for recordings and imaging. All chemicals for slicing preparation were purchased from Sigma.

For recordings, slices were submerged and perfused with ACSF at a rate of 3 ml/min at room temperature. Neurons were identified with differential interference contrast optics (Zeiss Examiner.Z1). The recording pipettes (3–4 MΩ) for whole-cell recording and cell-attached recording were pulled by a P-1000 glass pipette puller (Sutter Instrument). For whole-cell recordings, the pipettes were filled with internal solution that contained the following as reagent (in mM): 130 K-gluconate, 10 HEPES, 0.6 EGTA, 5 KCl, 3 Na₂ATP, 0.3 Na₃GTP, 4 MgCl₂ and 10 Na₂-phosphocreatine, (pH 7.2–7.4, 295–305 mOsm/L). For cell-attached recordings, ACSF was used as the intrapipette solution. Slice recordings were performed with MultiClamp 700B (Molecular Devices) and pClamp software. We conducted whole-cell recordings from 98 IPN neurons (85/98 in the rostral IPN and 13/98 in the central IPN). The neurons were held at –65 mV. The traces were low-pass filtered at 3 kHz and digitized at 10 kHz (Axon Digidata 1322A, Molecular Devices). The electrophysiological data were analyzed with Clampfit 10.2 software (Molecular Devices). We used the membrane test function in pClamp to measure membrane capacitance (C_m) and resistance (R_m). Membrane time constant (Tau) was determined by Tau = C_m * R_m (Isokawa, 1997). We determined the resting membrane potential of IPN neurons by subjecting neurons to 10 mV voltage steps and choosing the point of zero current from data interpolation.

For optogenetic stimulation, an optical fiber (0.2 mm core diameter, NA = 0.22) linked to a 473 nm laser driver (MBL-III-473, Changchun New Industries Optoelectronics Technology) was submerged in ACSF and placed ~0.3 mm from the recording site. The light intensity reaching the brain tissue was ~9 mW/mm².

The drugs were applied through perfusion by adding them to the ACSF following the dilution of a stock solution. The drug application onset indicates the switch in perfusion from standard ACSF to the drug-containing ACSF. The drugs include the following: baclofen (GABA_B agonist, 1 μ M; Sigma), picrotoxin (GABA_A antagonist, 50 μ M, Sigma), mecamylamine (Mec; nAChR antagonist, 5 μ M; Sigma), hexamethonium bromide (HMT; nAChR antagonist, 50 μ M; Sigma), and 6, 7-dinitroquinoline-2, 3-dione (DNQX; AMPA antagonist, 10 μ M; Sigma).

For two-photon imaging, brain slices containing the IPN were prepared, and oxygenated ACSF was continuously perfused at a rate of 3 ml/min at room temperature ($25 \pm 2^\circ\text{C}$). GCaMP6m fluorescent signals were imaged with a $20\times$ water immersion objective on a 2-photon microscope (FV1000, Olympus) at the rate of 1 Frame Per Second (FPS). We monitored the cholinergic axons in the IPN. To evoke Ca^{2+} transients, a bipolar electrode was placed in the IPN, and the electrical stimulation (1 ms per pulse, 50 or 100 μ A) at 10 Hz 1 s was applied for each test condition. The stimulation levels (50 or 100 μ A) were chosen to induce measurable Ca^{2+} signal changes within the imaging field in ACSF solution; they were comparable in WT mice and *KCTD8/12/16* triple KO mice (WT: 50 μ A for 5 fields and 100 μ A for 2 fields; triple KO: 50 μ A for 5 fields and 100 μ A for 1 field). Fluorescence intensities of GCaMP were measured with ImageJ software. We used two slices per mouse and chose 1–2 imaging fields per slice. In every field, we manually identified puncta as the regions of interest (ROIs) where Ca^{2+} signal showed increased response to electrical stimulation in ACSF. The intensities were then processed and plotted using a custom-written MATLAB program. We measured the area under the (peri-event) curve (AUC) between electrical stimulation onset (0 s) and peak Ca^{2+} signals (3 s) to represent the response strength to the baclofen treatment. ROIs size in WT mice and *KCTD8/12/16* KO mice was comparable.

Immunostaining and immunoblotting. Mice were deeply anesthetized with an overdose of pentobarbital and transcardially perfused with 0.9% saline, followed by paraformaldehyde (PFA, 4% w/v in PBS). Brains were removed and postfixed in 4% PFA for 4 h at room temperature. After samples were dehydrated in 30% sucrose solution, thin sections (35 μ m) were prepared on a cryostat microtome (Leica CM1950). For antigen retrieval, we incubated the sections with sodium citrate buffer solution (10 μ M; Sigma), adjusted to pH 6.0 with 1 M HCl at 95°C in a dry bath heater for 6 min (repeat twice with an interval of 15 min), then rinsed sections with PBS to cool down. After rinsing with 0.3% Triton X-100 in PBS (PBST) and blocking in 2% (w/v) BSA in PBST at room temperature for 1 h, the brain sections were incubated with primary antibodies anti-GABA_{B2} (1:200; catalog #G9920, Merck), anti-KCTD8 (1:200; catalog #ab110759, Abcam), anti-KCTD12 (1:200; catalog #15523-1-AP, Proteintech), anti-ChAT (choline acetyltransferase; 1:200; catalog #AB144P, Merck), and anti-Ca_v2.3 (1:200; catalog #C1853, Sigma) in the blocking solutions at 4°C for 48 h. After washing with PBS, the brain sections were incubated with fluorescent secondary antibodies (Cy2 or Cy3-conjugated donkey anti-goat, Cy2 or Cy3-conjugated goat anti-rabbit, Jackson ImmunoResearch) at room temperature for 2 h. Finally, PBS-washed sections were mounted with DAPI containing 50% glycerol. Fluorescent images were collected with a confocal microscope (Zeiss LSM880) or an automated fluorescent scanner (VS120Virtual Slide, Olympus). Images were analyzed and quantified using ImageJ.

For immunoblotting, protein extracts were prepared from the IPN of *KCTD8/12/16* KO or WT mice, lysed in a strong denaturing buffer containing 50 mM Tris-HCl, pH 7.6, 150 mM NaCl, 2 mM EDTA, 1% Triton X-100, 0.5% Sodium deoxycholate, 0.1% SDS, and a protease inhibitor cocktail (Roche Molecular Biochemicals) at 4°C . After sonication, soluble fraction was obtained by centrifugation at $130,000 \times g$ for 20 min at 4°C . Protein concentration was determined using the Pierce BCA Protein Assay Kit (Thermo Fisher Scientific). Protein extracts were denatured by the SDS loading buffer and boiled for 15 min. Then boiled samples were separated on a 4–20% SDS-PAGE gel before transfer to a PVDF membrane (Millipore) for further immunoblotting analysis. We used antibodies for KCTD8 and KCTD12 as mentioned above and other antibodies for KCTD16 (1:200; catalog #ab185104, Abcam) and α -tubulin (T8328-100UL, 1:30,000, SigmaAldrich).

Aversive conditioning, fiber photometry, and intra-IPN infusion. We used *KCTD8/12/16* KO, *KCTD8/12* KO, and WT mice for the behavioral

experiments. On day 0 (conditioning sessions), a mouse was placed into a conditioning chamber ($24 \times 24 \times 30$, L \times W \times H cm) with a metal fence floor and allowed to explore freely for 3 min. For fiber photometry experiments, 30 trials that consisted of footshock (0.6 mA scrambled, 0.5 s) delivered after an auditory tone (2 s, 7.5 kHz, 85–90 dB) with a 1 s delay were then conducted. For the intra-IPN drug injections, prolonged auditory tones (20 s, 7.5 kHz, 85–90 dB) were coupled to footshocks (0.7 mA scrambled, 1 s) and both stimuli coterminated for 10 trials. On days 1–3 (extinction sessions), mice were introduced into a new test chamber ($40 \times 30 \times 30$, L \times W \times H cm) that contained a white filter paper on the floor. Thirty or 10 auditory tones (same as the auditory tone for conditioning) were delivered after 2 min habituation without any footshock. Mice were returned to their home cages 3 min after the end of the last tone. Intertone intervals were randomly set between 30 and 50 s for fiber photometry experiments and 90–150 s for the intra-IPN drug injections.

For fiber photometry experiments, optical fiber implantation was conducted immediately after virus injection. A piece of optical fiber (catalog #FT200UMT, Thorlabs) was fit into a ceramic fiber ferrule (Shanghai Fiblaser). The optical fiber was implanted over the target brain areas with the tip 0.1 mm above the virus injection sites. The ceramic ferrule was supported with dental acrylic. All subsequent experiments were performed at least 3 weeks after virus injection to allow sufficient time for transgene expression and animal recovery. We recorded GCaMP signals using a fiber photometry system (ThinkerTech). We used an exciting beam from a 488 nm laser (0.01–0.02 mW; OBIS CORE 488LS; Coherent). The output signals were amplified and digitalized at 100 Hz. Auditory tone onset was used as the trigger event for data alignment. A custom MATLAB program and an Arduino R3 controller were used to generate the tone signal, and a Power 1401 digitizer simultaneously recorded tone timing and GCaMP signals (100 Hz sampling frequency). Fiber-photometry recording data were exported as MATLAB files from Spike2 software for further analysis. After smoothing the data with the MATLAB smooth function, we segmented the data based on behavioral events within individual trials. We derived the fluorescence change values by calculating the z score, where the baseline fluorescence signal was determined by averaging a 1.5 s long control time window 0.5 s before the cue initiation. The z score values are presented as heatmaps or as peri-event plots. The locomotion videos were analyzed using a custom-written MATLAB program. To examine the response strength of IPN neurons during the test sessions, we calculated the AUC of Ca^{2+} signal and locomotion for 3 s from conditioned stimuli onset (0 s) to represent the response in the aversion memory phase.

For the intra-IPN drug injections, a guide cannula (26 gauge, Plastics One) was implanted with its tip targeting the dorsal border of the IPN. After postsurgery recovery of 7 d, the mouse underwent the task of cued auditory fear conditioning. Before the extinction sessions in the following days, baclofen (15 pmol in 300 nl) or ACSF of equal volume was slowly infused into the IPN via the internal cannula (100 nl/min). Mice were allowed to rest 30 min to recover from the initial sedation. The mouse behavior was scored off-line by two trained observers without prior knowledge of mouse genotypes or drug treatments. Freezing was defined as the absence of movements, except for those related to respiration and slight head tremble. After the behavioral test, Texas Red conjugated dextran amine (MW = 3 kDa, catalog #D3328; Thermo Fisher Scientific) of equal volume (3%, 300 nl) was infused to the IPN via the cannula to identify the injection site and estimate the extent of the baclofen or ACSF injection.

Quantification and statistical analysis. We used MATLAB version 2019b, ImageJ 2.0.0, and GraphPad Prism 6 to perform the statistical analyses. For quantification of immunoreactivity, we manually identified the IPN regions of every slice as ROIs, and the signal intensity inside the ROIs were measured. To minimize the batch effects of the experiment repeats, we normalized the signal intensity of every section in different KCTD genotypes to the mean signal intensity of control mice in the same experimental batch (see Figs. 2A–D, 4B, WT mice) and mCherry-expressing control mice (see Fig. 5E,F). The precise statistical tests, exact p value, sample sizes (n) denoting the experimental replications, and the exact value of results are reported in the figure legends. All results were reported as means \pm SEM. Detailed statistical analyses are shown in Table 1.

Table 1. Summary of statistical analyses

Figure	Conditions	n Per group	Group 1 mean ± SEM	Group 2 mean ± SEM	Normality of distribution	Analysis	Factor	F(DFn,DFd)	Post hoc test/correction	p value					
1C	Basal	WT vs 3KO	11 (5),	66.3	20.1	62.8	15.1	Yes, yes	Two-way ANOVA	Genotype and drug	$F_{(1,819)} = 267.3$	N/A	<0.0001		
	Baclofen		12 (4)	1087.2	164.7	355.6	70.6	Yes, yes							
	Wash			79.8	15.0	79.6	27.4	Yes, yes							
1D	CHAT-ChR2 vs 3KO:CHAT-ChR2		11,15	-63.6	2.3	-61.6	1.4	Yes, yes	Unpaired t test	N/A	N/A	Welch's correction	0.4843		
	CHAT-ChR2 vs 3KO:CHAT-ChR2		8,13	44.1	5.6	36.6	4.3	Yes, no	Mann-Whitney test	N/A	N/A	N/A	0.1400		
	CHAT-ChR2 vs 3KO:CHAT-ChR2		8,13	268.0	28.8	318.4	38.0	Yes, yes	Unpaired t test	N/A	N/A	Welch's correction	0.3036		
	CHAT-ChR2 vs 3KO:CHAT-ChR2		8,13	11.1	1.3	10.7	1.5	Yes, no	Mann-Whitney test	N/A	N/A	N/A	0.7970		
1K	Basal		7 (3),	10.1	3.0	8.4	1.2	No, no	Mann-Whitney test	N/A	N/A	N/A	0.7984		
			6 (3)												
1L	Baclofen			93.9	10.2	59.5	7.7	No, no	Mann-Whitney test	N/A	N/A	N/A	0.0221		
2A	WT vs 3KO		22 (3),	1.00	0.04	1.01	0.03	Yes, yes	Unpaired t test	N/A	N/A	Welch's correction	0.7977		
			22 (3)												
2B	WT vs 3KO		25 (3),	1.00	0.06	0.91	0.04	Yes, yes	Unpaired t test	N/A	N/A	Welch's correction	0.2192		
			23 (3)												
2C	WT vs 3KO		25 (5),	1.00	0.03	0.72	0.04	Yes, yes	Unpaired t test	N/A	N/A	Welch's correction	<0.0001		
			25 (5)												
2D	WT vs 3KO		27 (3),	1.00	0.03	0.97	0.03	Yes, yes	Unpaired t test	N/A	N/A	Welch's correction	0.4149		
			29 (3)												
2F	WT	Basal vs Baclofen	9 (2)	3.1	0.8	1.0	0.7	Yes, yes	Paired t test	Two-way ANOVA	Genotype and drug	$F_{(1,42)} = 2.113$	N/A	0.0064	0.1535
		Baclofen vs Wash		1.0	0.7	3.5	1.0								
	3KO	Basal vs Baclofen	7 (3)	4.6	0.6	1.4	0.4		Paired t test					0.0028	
		Baclofen vs Wash		1.4	0.4	4.1	0.4		Paired t test					0.0008	
4B	WT vs KCTD8/12 KO		30 (6),	1.00	0.03	0.78	0.02	Yes, yes	One-way ANOVA	Genotype	$F_{(4,107)} = 9.392$	Sidak's multiple comparisons test	<0.0001	<0.0001	
	WT vs KCTD8 KO		30 (6),		0.98	0.04	Yes, yes								
	WT vs KCTD12 KO		30 (6),		0.89	0.04	Yes, yes								
	WT vs KCTD16 KO		30 (6),		0.90	0.03	Yes, yes								
4C	CHAT-ChR2 vs KCTD8/12 KO:CHAT-ChR2		13 (5),	112.9	44.7	104.4	37.4	Yes, yes	Two-way ANOVA	Genotype and drug	$F_{(4,116)} = 2.185$	Sidak's multiple comparisons test	0.075	0.029	
			7 (3)	1152.6	177.1	455.7	128.3								
	CHAT-ChR2 vs KCTD8 KO:CHAT-ChR2		13 (5),		94.9	43.9	66.2	27.2	Yes, yes					0.4395	
			7 (3)			738.8	156.9	104.3	25.9						
	CHAT-ChR2 vs KCTD12 KO:CHAT-ChR2		13 (5),			80.6	30.2	Yes, yes						0.2295	
			9 (3)			723.9	101.7	98.9	28.4						
	CHAT-ChR2 vs KCTD16 KO:CHAT-ChR2		13 (5),			133.8	74.3	Yes, yes						0.9846	
			8 (3)			957.2	284.8	175.1	99.6						
5E	mCherry- vs KCTD8-		14 (2),	1.00	0.05	1.41	0.04	Yes, yes	Unpaired t test	N/A	N/A	Welch's correction	<0.0001		
5F	mCherry- vs KCTD12-		21 (3),	1.00	0.02	1.19	0.04	Yes, yes	Unpaired t test	N/A	N/A	Welch's correction	0.0002		
5G	mCherry- vs KCTD8-		17 (4),	45.6	8.9	65.6	17.0	Yes, yes	Two-way ANOVA	Genotype and drug	$F_{(2,58)} = 5.669$	Sidak's multiple comparisons test	0.0056	0.0290	
	mCherry- vs KCTD12-		7 (3)	567.3	113.3	1179.5	90.9	Yes, yes							
6E	WT	Trials 1–5 vs 6–10	6	6.11	2.11	4.28	2.15	Yes, yes	Two-way ANOVA	Genotype and trial	$F_{(1,60)} = 20.09$	Sidak's multiple comparisons test	<0.0001	0.9878	
		Trials 1–5 vs 11–15				5.88	2.44	Yes, yes							
		Trials 1–5 vs 16–20				4.97	2.91	Yes, yes							
		Trials 1–5 vs 21–25				4.39	2.51	Yes, yes							
		Trials 1–5 vs 26–30				4.42	2.58	Yes, yes							
	3KO	Trials 1–5 vs 6–10	7	12.16	2.54	10.18	1.60	Yes, yes					>0.9999		
		Trials 1–5 vs 11–15				10.35	1.93	Yes, yes					0.9999		
		Trials 1–5 vs 16–20				10.72	1.49	Yes, yes					>0.9999		
		Trials 1–5 vs 21–25				10.66	1.92	Yes, yes					>0.9999		
		Trials 1–5 vs 26–30				11.33	2.55	Yes, yes					0.9969		

(Table continues.)

Table 1 Continued

Figure	Conditions	n Per group	Group 1 mean ± SEM	Group 2 mean ± SEM	Normality of distribution	Analysis	Factor	F(DFn,DFd)	Post hoc test/correction	p value		
6F	Conditioning	WT vs 3KO	2.95	0.94	3.89	1.07	Yes, yes	Two-way ANOVA	Genotype and trial	$F_{(1,66)} = 2.977$	N/A	0.0909
			6.31	3.19	6.64	1.33						
			4.94	2.65	9.76	3.40						
			5.18	2.31	8.40	1.79						
			6.04	1.51	8.68	1.05						
			6.63	2.15	9.81	2.78						
	Extinction day 1	4.45	0.73	6.41	1.27	Yes, yes	Two-way ANOVA	Genotype and trial	$F_{(1,66)} = 14.72$	N/A	0.0003	
		4.22	1.52	7.56	2.34							
		1.79	1.39	8.79	2.19							
		1.81	0.88	4.80	1.87							
		1.52	1.03	4.28	1.54							
		2.31	1.00	5.55	1.69							
	Extinction day 2	1.04	0.70	7.67	3.28	Yes, yes	Two-way ANOVA	Genotype and trial	$F_{(1,66)} = 12.28$	N/A	0.0008	
		0.11	0.76	5.02	2.65							
		-0.67	1.48	4.71	1.92							
		0.86	2.01	3.46	1.63							
		0.92	1.98	2.77	1.86							
		1.32	1.99	5.16	2.10							
	Extinction day 3	1.11	1.25	2.92	1.23	Yes, yes	Two-way ANOVA	Genotype and trial	$F_{(1,66)} = 5.460$	N/A	0.0225	
		-0.82	1.67	4.02	1.50							
		0.68	0.73	1.18	1.46							
		1.22	1.12	1.40	1.37							
		0.45	1.17	1.46	1.35							
		1.53	1.00	2.52	0.92							
WT	Day 1 vs day 2	6	4.45	0.73	1.04	0.70	Yes, yes	Two-way ANOVA	Extinction day and trial	$F_{(1,66)} = 6.876$	N/A	0.0111
			4.22	1.52	0.11	0.76						
			1.79	1.39	-0.67	1.48						
			1.81	0.88	0.86	2.01						
			1.52	1.03	0.92	1.98						
			2.31	1.00	1.32	1.99						
	Day 1 vs day 3	1.11	1.25	1.11	1.25	Yes, yes	Two-way ANOVA	Extinction day and trial	$F_{(1,66)} = 8.843$	N/A	0.0042	
		-0.82	1.67	-0.82	1.67							
		0.68	0.73	0.68	0.73							
		1.22	1.12	1.22	1.12							
		0.45	1.17	0.45	1.17							
		1.53	1.00	1.53	1.00							
3KO	Day 1 vs day 2	7	6.41	1.27	7.67	3.28	Yes, yes	Two-way ANOVA	Extinction day and trial	$F_{(1,72)} = 1.405$	N/A	0.2398
			7.56	2.34	5.02	2.65						
			8.79	2.19	4.71	1.92						
			4.80	1.87	3.46	1.63						
			4.28	1.54	2.77	1.86						
			5.55	1.69	5.16	2.10						
	Day 1 vs day 3	2.92	1.23	2.92	1.23	Yes, yes	Two-way ANOVA	Extinction day and trial	$F_{(1,72)} = 16.86$	N/A	0.0001	
		4.02	1.50	4.02	1.50							
		1.18	1.46	1.18	1.46							
		1.40	1.37	1.40	1.37							
		1.46	1.35	1.46	1.35							
		2.52	0.92	2.52	0.92							
6G	Conditioning	WT vs 3KO	6.86	1.92	4.30	0.99	Yes, yes	Two-way ANOVA	Genotype and trial	$F_{(1,66)} = 5.346$	N/A	0.0240
			9.04	3.81	3.04	0.82						
			5.60	2.84	2.49	0.72						
			4.30	1.99	1.88	0.24						
			6.21	2.79	2.32	0.31						
			5.99	3.49	5.85	1.73						
	Extinction day 1	12.91	3.02	3.58	1.87	Yes, yes	Two-way ANOVA	Genotype and trial	$F_{(1,66)} = 21.70$	N/A	<0.0001	
		16.29	4.51	3.28	1.32							
		23.47	9.09	4.99	2.19							
		28.84	7.37	8.05	0.81							
		33.50	7.84	12.07	3.60							
		35.28	13.57	15.77	2.50							

(Table continues.)

Table 1 Continued

Figure	Conditions	n Per group	Group 1 mean ± SEM	Group 2 mean ± SEM	Normality of distribution	Analysis	Factor	F(DFn,DFd)	Post hoc test/correction	p value			
6H	Extinction day 2		21.46	5.45	14.85	11.45	Yes, yes	Two-way ANOVA	Genotype and trial	$F_{(1,66)} = 5.088$	N/A	0.0277	
			19.82	7.42	19.06	9.91							
			32.44	9.83	16.46	4.70							
			34.65	9.26	20.13	3.81							
			44.22	10.75	28.80	9.07							
			34.17	14.91	25.15	7.01							
	Extinction day 3			13.24	2.25	24.85	6.56	Yes, yes	Two-way ANOVA	Genotype and trial	$F_{(1,66)} = 4.581$	N/A	0.0365
				28.49	6.99	13.31	4.36						
				27.93	13.27	14.59	4.13						
				31.76	9.70	24.58	5.71						
				39.72	13.31	21.01	4.32						
				31.60	9.33	15.13	5.57						
	7C WT	Conditioning ACSF vs Baclofen	8,6	42.9	3.5	68.2	8.6	Yes, yes	Unpaired t test	N/A	N/A	Welch's correction	0.0306
				7,6	1.00	0.61	0.39						
	7C	Extinction day 1		3.55	1.03	2.38	0.88	Yes, yes	Two-way ANOVA	Genotype and drug	$F_{(1,110)} = 101.5$	N/A	<0.0001
				9.65	1.25	8.86	1.17						
				9.66	1.35	9.44	0.69						
				11.08	1.48	10.51	1.10						
13.44				0.90	12.04	0.99							
15.39				1.01	14.83	0.28							
Extinction day 2				14.36	0.96	13.62	0.50	Yes, yes	Two-way ANOVA	Genotype and drug	$F_{(1,110)} = 122.6$	N/A	<0.0001
				15.26	0.97	14.12	0.55						
				14.57	1.14	13.79	1.13						
				16.88	0.37	12.57	0.97						
				17.07	0.71	13.18	1.28						
				17.49	0.41	13.88	1.62						
Extinction day 3				17.73	0.45	11.30	2.17	Yes, yes	Two-way ANOVA	Genotype and drug	$F_{(1,110)} = 15.91$	N/A	0.0001
				15.63	0.79	11.13	0.94						
				15.94	1.40	11.74	0.98						
				16.54	0.55	9.34	1.29						
				15.08	1.20	9.06	1.82						
				15.93	1.07	9.44	1.33						
KCTD8/12 KO	Conditioning ACSF vs Baclofen	6,6	14.11	1.49	7.83	1.40	Yes, yes	Two-way ANOVA	Genotype and drug	$F_{(1,100)} = 1.510$	N/A	0.2221	
			14.24	0.79	10.20	2.07							
			13.59	1.01	5.80	0.99							
			11.05	1.23	4.60	1.27							
			11.57	1.60	3.84	1.61							
			12.18	0.92	4.80	1.95							
			10.54	0.93	3.01	1.21							
			8.45	0.83	3.14	1.23							
			9.19	1.14	3.26	1.50							
			8.56	0.96	3.99	1.32							
			7.67	0.95	2.09	1.22							
			7.45	1.04	4.04	1.49							
4.40	0.97	3.97	1.08										
4.64	1.25	3.20	1.27										
6.48	1.09	2.47	0.76										
5.19	1.25	1.89	0.84										
3.04	1.18	1.68	0.54										
4.04	1.38	1.93	1.03										
2.75	1.16	0.38	0.16										
2.82	0.49	2.63	2.25										
4.52	1.92	1.73	0.77										
1.51	0.42	1.99	0.64										
2.53	0.46	4.61	1.14										
7.40	1.58	8.27	1.81										
88.57	1.68	11.49	0.43										
10.87	1.63	11.83	1.50										
12.76	1.35	12.60	1.88										
10.49	2.44	13.46	1.64										
12.66	1.78	11.20	2.22										
14.58	1.28	11.61	1.74										
10.06	1.70	12.82	1.37										

(Table continues.)

Table 1 Continued

Figure	Conditions	n Per group	Group 1 mean ± SEM	Group 2 mean ± SEM	Normality of distribution	Analysis	Factor	F(DFn,DFd)	Post hoc test/correction	p value		
	Extinction day 1		13.50	11.84	Yes, yes	Two-way ANOVA	Genotype and drug	$F_{(1,100)} = 5.375$	N/A	0.0225		
			1.33	1.71								
			15.61	13.17								
			1.21	1.57								
			13.16	12.20								
			1.13	0.75								
			15.48	13.41								
			1.26	1.74								
			12.29	14.85								
			1.73	1.22								
			12.38	12.88								
			2.39	1.53								
			15.47	8.85								
	1.26	1.37										
	11.12	10.98										
	1.98	1.06										
	11.87	10.35										
	1.18	1.15										
	13.10	10.58										
	0.89	1.23										
	Extinction day 2		11	1.50	Yes, yes	Two-way ANOVA	Genotype and drug	$F_{(1,100)} = 25.25$	N/A	<0.0001		
			0.87									
			7.45									
			1.50									
			0.12	1.48								
			1.64	1.38								
			11.59	6.00								
			1.90	1.25								
			10.56	6.45								
			1.72	1.19								
			10.82	6.66								
			2.28	1.19								
			9.39	4.18								
	1.61	1.24										
	10.20	6.01										
	2.04	1.67										
	6.72	4.00										
	1.00	0.77										
	6.27	3.75										
	1.94	1.35										
	6.59	4.49										
	1.49	0.85										
	7.12											
	Extinction day 3		6.30	1.42	Yes, yes	Two-way ANOVA	Genotype and drug	$F_{(1,100)} = 1.542$	N/A	0.2175		
			1.90									
			3.51									
			1.42									
			3.34	1.03								
			0.93	1.03								
			3.14	0.88								
			0.78	0.88								
			4.24	0.75								
			0.94	0.75								
			4.19	1.20								
			1.45	1.20								
			4.91	2.21								
	2.09	1.00										
	3.62	3.47										
	0.67	1.14										
	3.35	1.05										
	1.03	1.05										
	3.13	0.92										
	0.71	0.92										
	1.37	0.76										
	0.68	0.76										
7D WT	Conditioning	ACSF vs Baclofen	7,6	108.95	2.85	Yes, yes	One-way ANOVA	Drug	$F_{(7,44)} = 55.41$	Tukey's multiple comparisons test	<0.0001	0.9828
				5.45	2.85							
				99.89	2.85							
				2.85								
	Extinction day 1			162.41	9.43	Yes, yes						<0.0001
	Extinction day 2			107.14	10.23	Yes, yes						<0.0001
	Extinction day 3			45.33	5.12	Yes, yes						0.3578
7D KCTD8/12 KO	Conditioning	ACSF vs Baclofen	6,6	91.43	9.77	Yes, yes	One-way ANOVA	Drug	$F_{(7,40)} = 16.20$	Tukey's multiple comparisons test	<0.0001	0.9978
				10.91	9.77							
				99.88	9.77							
				9.77								
	Extinction day 1			133.98	7.99	Yes, yes						0.9418
	Extinction day 2			90.39	10.74	Yes, yes						0.1920
	Extinction day 3			37.59	7.72	Yes, yes						0.9997
	7E	WT vs KCTD8/12 KO	8,6	16.4	1.7	Yes, yes	Unpaired t test	N/A	N/A	Welch's correction	0.9001	

N/A: Not applicable.

Results

Triple KO of *KCTD8/12/16* reduces GABA_B presynaptic excitation

We first analyzed the effect of knocking out *KCTD8/12/16* on GABA_B receptors–mediated potentiation of the glutamate release from the MHb terminals. Our previous studies have shown that brief photostimulation of the so-called cholinergic habenula neurons in *ChAT-ChR2* mice evokes rapid glutamate release, whereas prolong stimulation leads to slow volume transmission of acetylcholine (Ren et al., 2011; Hu et al., 2012; Zhang et al., 2016). By crossing the *KCTD8/12/16* KO mice with the *ChAT-ChR2* mice, we performed whole-cell recordings from IPN neurons to examine glutamatergic EPSCs on brief stimulation of ChR2-expressing axonal terminals (Fig. 1A). To isolate glutamate currents, we applied a blocker cocktail solution comprising picrotoxin, HMT, and Mec to inhibit GABA_A receptors and nicotinic acetylcholine receptors (Ren et al., 2011; Zhang et al., 2016).

We observed a strong decrease in GABA_B-mediated presynaptic excitation in the *KCTD8/12/16* triple knock-out mice. In the control *ChAT-ChR2* mice, GABA_B receptors agonist (1 μM

baclofen) produced a striking increase in the amplitude of light-evoked EPSCs (Fig. 1B,C). In *KCTD8/12/16* KO::*ChAT-ChR2* mice, terminal stimulation produced similarly small inward currents, which was also potentiated by baclofen (Fig. 1B,C). However, compared with the control *ChAT-ChR2* mice, baclofen-induced potentiation of EPSCs was significantly reduced in *KCTD8/12/16* KO::*ChAT-ChR2* mice (67.3% reduction in fold increase; Fig. 1C). We note that the intrinsic properties (e.g., resting membrane potential, membrane capacitance, resistance, and membrane time constant) of IPN neurons were not altered in the *KCTD8/12/16* KO mice (Fig. 1D). These results suggest that *KCTD8*, *12*, and *16* are involved in the GABA_B receptors–mediated potentiation of glutamate release from the MHb.

As GABA_B receptors are known to exert excitation via amplifying presynaptic Ca²⁺ entry through Ca_{v2.3} channels (Zhang et al., 2016), we next tested whether *KCTD8/12/16* KO had an effect on Ca²⁺ entry into the MHb axonal terminals. We used recombinant AAV vectors to express a genetically encoded Ca²⁺ indicator (GCaMP6m) in MHb neurons and measured GCaMP fluorescence changes from the MHb axonal terminals within the

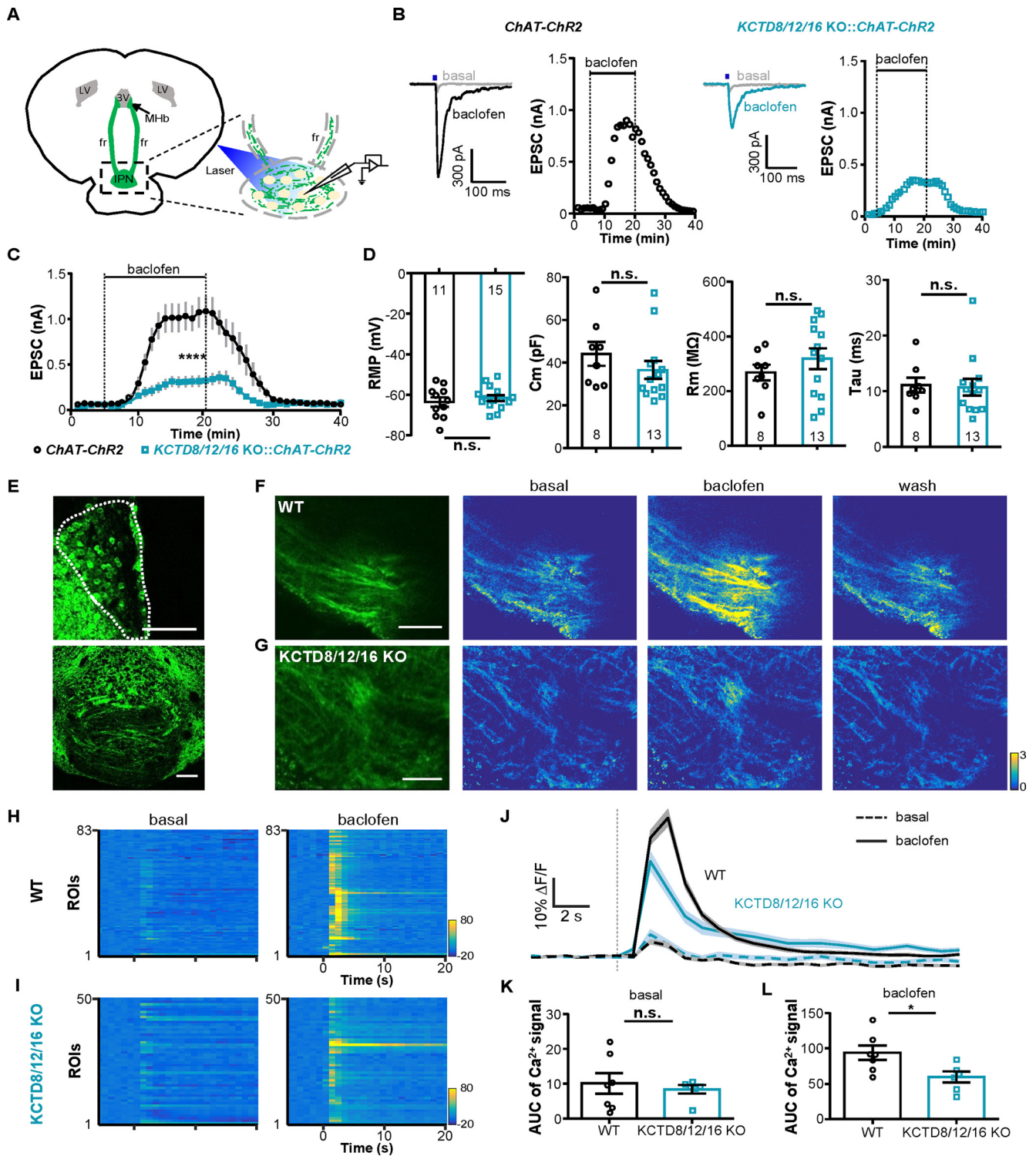


Figure 1. Triple KO of *KCTD8/12/16* reduces the GABA_B receptors–mediated potentiation of synaptic glutamate release and Ca²⁺ entry of MHB terminals. **A**, The schematic shows the habenulo–interpeduncular pathway in a coronal section and the recording from IPN neurons in response to photostimulation of ChR2-expressing axonal terminals. **B**, In IPN neurons of *ChAT-ChR2* (left) and *KCTD8/12/16 KO::ChAT-ChR2* (right) mice, a brief pulse of photostimulation (5 ms duration, 473 nm) of MHB cholinergic terminals elicited glutamatergic EPSCs that were potentiated by the GABA_B agonist baclofen (1 μM). Raw traces and time-series plots are shown. Gray indicates basal responses, and black and blue indicate responses in baclofen application in the two mouse lines. EPSCs were recorded in the presence of a cocktail solution comprising GABA_A blocker (50 μM picrotoxin) and nAChR blockers (50 μM HMT and 5 μM Mec). **C**, Averaged time-series plot of EPSC amplitudes to compare the baclofen-induced potentiation between *ChAT-ChR2* mice ($I_{\text{Basal}} = 66.3 \pm 20.1$ pA; $I_{\text{Baclofen}} = 1087.2 \pm 164.7$ pA; $n = 11$ cells from 5 mice) and *KCTD8/12/16 KO::ChAT-ChR2* mice ($I_{\text{Basal}} = 62.8 \pm 15.1$ pA; $I_{\text{Baclofen}} = 355.6 \pm 70.6$ pA; $n = 12$ cells from 4 mice). **** $p < 0.0001$; Two-way ANOVA test for the difference of EPSCs between *ChAT-ChR2* and *KCTD8/12/16 KO::ChAT-ChR2* mice. **D**, Comparison of resting membrane potentials (RMP; WT: -63.6 ± 2.3 mV, $n = 11$; 3KO: -61.6 ± 1.4 mV, $n = 15$), Cm (WT: 44.1 ± 5.6 pF, $n = 8$; 3KO: 36.6 ± 4.3 pF, $n = 13$), Rm (WT: 268.0 ± 28.8 MΩ, $n = 8$; 3KO: 318.4 ± 38.0 MΩ, $n = 13$), and Tau (WT: 11.1 ± 1.3 , $n = 8$; 3KO: 10.7 ± 1.5 , $n = 13$) of IPN neurons recorded from *ChAT-ChR2* and *KCTD8/12/16 KO::ChAT-ChR2* mice. n.s., Not significant. Unpaired *t* test and Mann–Whitney test (with Welch’s correction). Each dot indicates an individual cell, and the number of dots indicate sample size. **E**, Example images show AAV transduction of GCaMP6m in MHB neurons (top) and expression of GCaMP6m in the axonal terminals within the IPN (bottom) of WT mice and *KCTD8/12/16 KO* mice. **F**, **G**, Two-photon imaging of GCaMP6m fluorescence changes in the habenular terminals within the IPN of WT mice (**F**) and *KCTD8/12/16 KO* mice

IPN brain sections using two-photon microscopy (Fig. 1E). Baclofen strongly increased presynaptic Ca²⁺ signals following electrical stimulation (10 pulses at 10 Hz) in wild-type (WT) C57BL/6N mice (Fig. 1F,H). Similarly, baclofen increased presynaptic Ca²⁺ signals in *KCTD8/12/16* KO mice (Fig. 1G,I), suggesting that *KCTD8/12/16* KO mice maintained GABA_B receptors–mediated amplifying Ca²⁺ entry of the MHb axonal terminals. Compared with WT mice, we found that changes of Ca²⁺ signals following electrical stimulation showed no difference without baclofen but were significantly reduced after the application of baclofen in *KCTD8/12/16* KO mice (36.6% difference in baclofen-mediated fold increase; Fig. 1J–L). These results thus demonstrated that *KCTD8/12/16* KO reduced GABA_B receptors–mediated presynaptic Ca²⁺ entry of the MHb axonal terminals. Our results collectively indicated that the genetic deficiency of *KCTD8/12/16* reduced GABA_B receptors–mediated presynaptic excitation.

KCTD8/12/16 KO reduces GABA_B receptors expression in MHb axonal terminals

Previous studies have shown that KCTDs interact with GABA_B receptors and with Ca_{v2.3} (Gassmann and Bettler, 2012; Bhandari et al., 2021). We explored whether *KCTD8/12/16* KO influenced axonal expression of Ca_{v2.3} and GABA_B receptors by immunostaining of IPN brain sections. We did not detect any significant changes in the expression of Ca_{v2.3} in the MHb axonal terminals between WT and *KCTD8/12/16* KO mice (Fig. 2A). Also, the immunoreactivity of choline acetyltransferase (ChAT)—a marker of cholinergic neurons—was unaltered in the MHb axonal terminals of *KCTD8/12/16* KO mice (Fig. 2B). Surprisingly, the expression of GABA_{B2} receptor subunit was significantly reduced in the MHb axonal terminals within the IPN in *KCTD8/12/16* KO mice (Fig. 2C). Knocking out *KCTD8/12/16* did not change the level of GABA_{B2} expression in the MHb, where the somata and dendrites of MHb neurons are located (Fig. 2D).

Next, we conducted cell-attached recordings from MHb neurons to test whether knocking out *KCTD8/12/16* influenced the function of GABA_B receptors in the somata of MHb neurons. Baclofen significantly reduced the firing rates of the MHb neurons in both WT and *KCTD8/12/16* KO mice (Fig. 2E,F). There was no difference in the baseline firing rates and the effects of GABA_B-mediated inhibition between WT and *KCTD8/12/16* KO mice (Fig. 2F), indicating that *KCTD8*, *12*, and *16* do not have an obvious effect on GABA_B-mediated inhibitory responses in the somata of MHb neurons.

These results thus suggested that certain isoforms of *KCTD8/12/16*, either functioning separately or in combination, regulate

the expression of GABA_B receptors in the axonal terminals but not somata/dendrites of habenula cholinergic neurons.

KCTD8 and 12 are important for presynaptic GABA_B expression and signaling

Given the physiological and neurochemistry phenotypes of the triple knock-out mice, we asked which of these three KCTD proteins might be involved in the axonal expression and presynaptic excitation of GABA_B receptors. We examined the expression of KCTD isoforms in the cholinergic pathway from the MHb to the IPN. Immunohistochemistry revealed strong *KCTD8* expression and moderate *KCTD12* expression in the somata and axonal terminals of ChAT-expressing habenula cells (Fig. 3A–D). The immunoreactivity was absent in the *KCTD8/12/16* triple KO mice (Fig. 3E–G), which confirmed the validity of our antibodies. These observations are also consistent with the mRNA *in situ* hybridization data in the Allen Brain Atlas (Fig. 3H). The *KCTD16* antibody was not appropriate for immunohistochemistry, but *KCTD16* mRNA level was very low in the MHb according to the Allen Brain Atlas (Fig. 3H). Altogether, these results demonstrated that *KCTD8* and *KCTD12* rather than *KCTD16* were expressed in habenula cholinergic neurons.

We tested the isoform-specific contribution of KCTDs by analyzing the immunoreactivities of GABA_{B2} receptor subunit in the cholinergic terminals within the IPN of *KCTD8* KO, *KCTD12* KO, and *KCTD16* KO mice. We observed no significance difference in the GABA_{B2} immunoreactivity of the axonal terminals within the IPN between the WT mice and the single knock-out mice, but a significant decrease of the GABA_{B2} immunoreactivity in *KCTD8/12* double KO mice (Fig. 4A,B).

We crossed various *KCTD* KO genotypes mice with *ChAT-ChR2-EYFP* mice and performed whole-cell recordings from IPN neurons to examine any potential changes in the baclofen-induced potentiation of EPSCs. In accordance with the reduced axonal GABA_B receptors expression in *KCTD8/12* KO mice, we observed impaired baclofen-induced potentiation of EPSCs (60.5% reduction; Fig. 4C). As expected, single *KCTD* KO showed no difference in baclofen-induced potentiation of EPSCs with *ChAT-ChR2* mice (Fig. 4C). Altogether, these experiments thus revealed that both *KCTD8* and *KCTD12* are important for facilitating the expression and presynaptic excitation of GABA_B receptors in the axonal terminals of habenula cholinergic neurons.

The phenotypes of knocking out both *KCTD8* and *KCTD12* suggest that (1) both isoforms critically contribute to presynaptic signaling possibly by forming KCTD hetero-oligomers, or (2) either isoform is dispensable and the total expression levels of the two isoforms are important. We tested the two hypotheses by overexpressing a single KCTD in the habenula neurons of *KCTD8/12/16* KO mice. We infused AAV to express mCherry, *KCTD8*-mCherry, or *KCTD12*-mCherry into the MHb of the triple KO mice and examined the axonal expression and presynaptic excitation of GABA_B receptors. AAV transduction produced strong expression of *KCTD8* or *KCTD12* (Fig. 5A,C). Compared with mCherry-expression controls, overexpressing either *KCTD8* or *KCTD12* significantly increased the axonal expression of GABA_B receptors (Fig. 5B,D–F) and baclofen-induced potentiation of EPSCs (Fig. 5G). Therefore, overexpressing either *KCTD8* or *KCTD12* alone is sufficient to facilitate the presynaptic expression and signaling of GABA_B receptors in habenula cholinergic neurons.

←

(G). Left, Example image shows the GcAMP6 expression in the IPN. Right, Pseudocolor images show the GcAMP6 signal changes within the same area by application of the baclofen (1 μM) following electrical stimulation (10 pulses at 10 Hz). H, I, Heatmaps illustrate that baclofen increased GcAMP6 signals for 83 terminal areas of WT mice (7 imaging fields from 3 mice) and 50 terminal areas of *KCTD8/12/16* KO mice within (6 imaging fields from 3 mice). J, Average GcAMP6 signals from WT (black) and *KCTD8/12/16* KO (blue) mice following electrical stimulations. Dashed line indicates basal, solid line indicates baclofen, and shaded area indicates SEM. K, L, Comparison of AUC of GcAMP signals (from electrical stimulation onset, *t* = 0 s, to peak GcAMP6 signals, *t* = 3 s) between WT and *KCTD8/12/16* triple KO mice during baseline condition (WT, 10.1 ± 3.0; 3KO, 8.4 ± 1.2; K) and in the presence of baclofen (WT, 93.9 ± 10.2; 3KO, 59.5 ± 7.7; L). Number of individual dots indicate the sample size. n.s., Not significant. **p* < 0.05; Mann–Whitney tests. Data are presented as means ± SEM (Table 1). Scale bars: E–G, 100 μm.

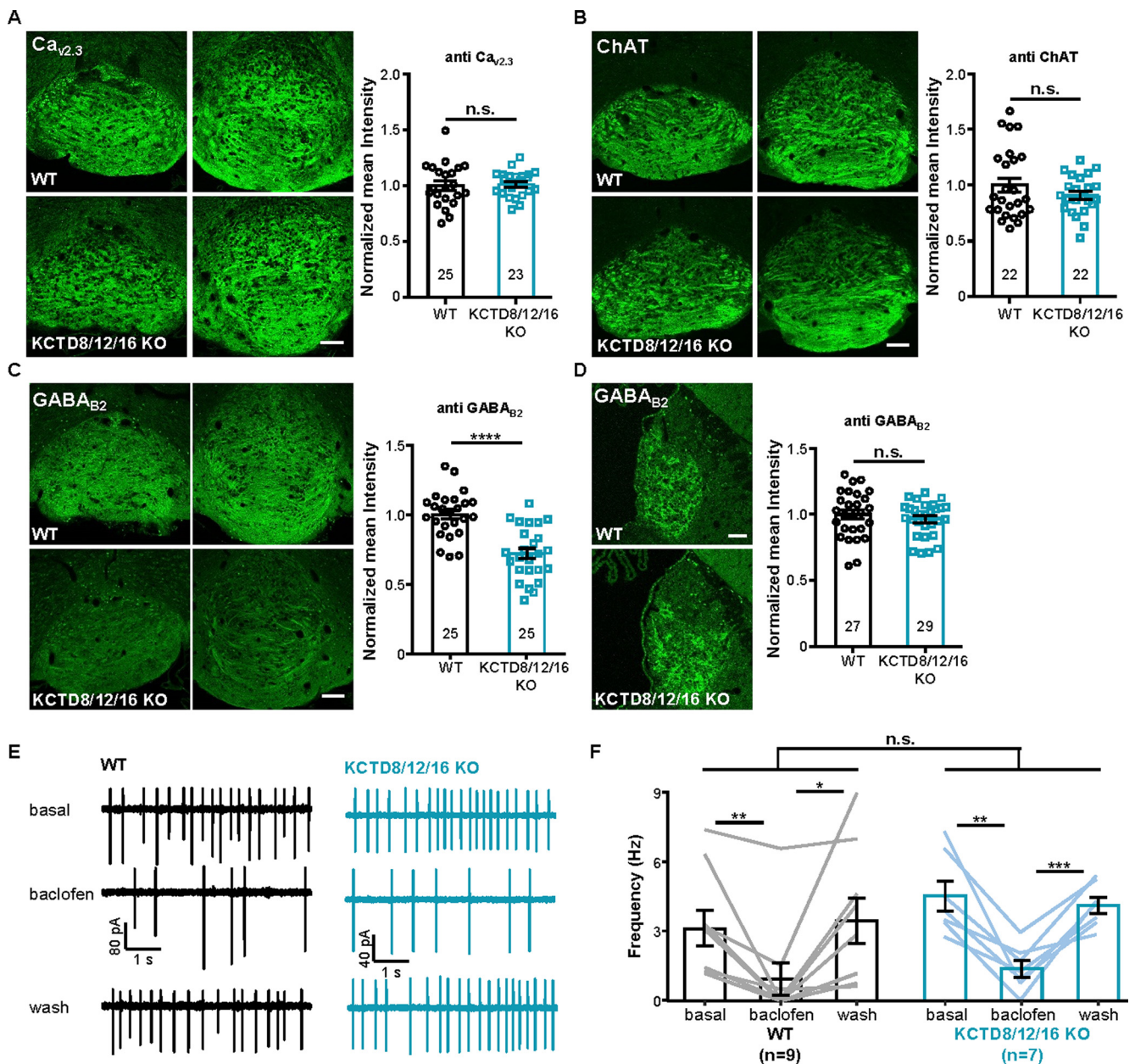


Figure 2. The effects of *KCTD8/12/16* KO on the expression of Cav_{2.3}, ChAT, and GABA_{B2} in the axonal terminals of MHB neurons. **A**, Images show the immunoreactivity of Cav_{2.3} in the anterior and posterior brain sections of the IPN of WT mice (top) and *KCTD8/12/16* KO mice (bottom). Right, Bar plot shows the summary data of the normalized mean pixel intensity of Cav_{2.3} immunoreactivity (WT: 1.00 ± 0.04, *n* = 22 slices from 3 mice; 3KO: 1.01 ± 0.03, *n* = 22 slices from 3 mice). n.s., Not significant. Unpaired *t* test (with Welch's correction). **B**, Images and summary plot show the ChAT immunoreactivity within the IPN of WT mice and *KCTD8/12/16* KO mice (WT: 1.00 ± 0.06, *n* = 25 slices from 3 mice; 3KO: 0.91 ± 0.04, *n* = 23 slices from 3 mice). Same conventions as in **A**. **C**, Images and summary plot show significantly lower GABA_{B2} immunoreactivity within the IPN of *KCTD8/12/16* KO mice (WT: 1.00 ± 0.03, *n* = 25 slices from 5 mice; 3KO: 0.72 ± 0.04, *n* = 25 slices from 5 mice). *****p* < 0.0001; unpaired *t* test (with Welch's correction). **D**, Images and summary plot show no difference in GABA_{B2} immunoreactivity in the soma area of MHB neurons between WT and *KCTD8/12/16* KO mice (WT: 1.00 ± 0.03, *n* = 27 slices from 3 mice; 3KO: 0.97 ± 0.03, *n* = 29 slices from 3 mice). n.s., Not significant. Unpaired *t* test (with Welch's correction). **E**, Raw traces of cell-attached recordings show the action potential firing of MHB neurons before, during, and after baclofen (1 μM) in the presence of a cocktail solution comprising DNQX, picrotoxin, HMT, and Mec. Left, WT mice. Right, *KCTD8/12/16* KO mice. **F**, Group data show that firing rates of MHB neurons are reversibly inhibited by baclofen in WT (*n* = 9 cells) and *KCTD8/12/16* KO (*n* = 7 cells) mice. **p* < 0.05, ***p* < 0.01, ****p* < 0.001; paired *t* test for difference between basal and baclofen and between baclofen and wash. Two-way ANOVA for the difference between WT and *KCTD8/12/16* KO mice. Data are presented as means ± SEM (Table 1). Scale bars, **A–D**, 100 μm.

KCTDs regulate neuronal responses to aversion-predicting cues

Given that GABA_B-mediated presynaptic excitation in the MHB–IPN pathway regulates aversive memory expression (Soria-Gómez et al., 2015; Zhang et al., 2016), we examined the involvement of KCTDs in the cued-aversion response. We trained mice with an aversive pavlovian conditioning paradigm by presenting a 2 s auditory tone [conditioned stimulus (CS)]

with the delayed (1 s) delivery of a brief footshock [0.5 s; unconditioned stimulus (US); Lu et al., 2020]. We expressed GCaMP6m in the IPN neurons—the downstream of habenula cholinergic neurons—and implanted an optical fiber with its tip in the IPN for fiber photometry of GCaMP fluorescence changes during the conditioning sessions (Fig. 6A,B).

Initially, the US but not the CS induced Ca²⁺ transients at the population level in both WT and *KCTD8/12/16* KO mice.

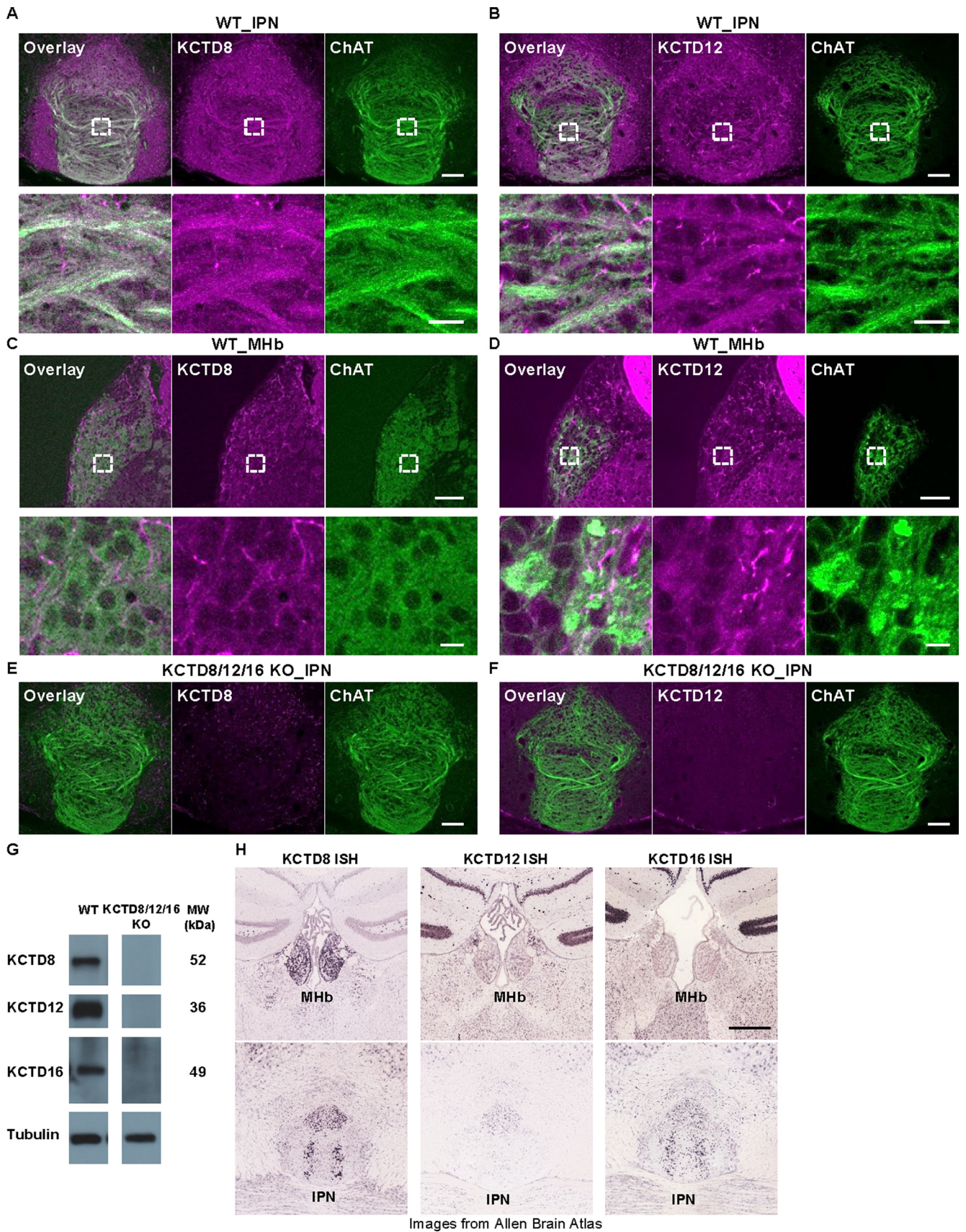


Figure 3. Distributions of KCTDs in the habenulo–interpeduncular cholinergic pathway. **A, B**, Images show the colocalizations of KCTD8 (**A**) or KCTD12 (**B**) with ChAT in the IPN of a WT mouse. Top, The immunoreactivities of KCTD8 or KCTD12 (magenta) and ChAT (green). Bottom, zoomed-in views of the dashed rectangular areas. **C, D**, Images show the distribution of KCTD8 (**C**) or KCTD12 (**D**) in the MHb of a WT mouse. Top, The immunoreactivities of KCTD8 (magenta) and ChAT (green). Bottom, Zoomed-in view of the dashed rectangular area. **E, F**, Images show the immunoreactivities of KCTD8 (magenta, **E**), KCTD12 (magenta, **F**) and ChAT (green) in the IPN of a *KCTD8/12/16* KO mice. **G**, Immunoblotting show the presence of KCTD8, 12, and 16 in

Within trials 3–5, the CS began to induce an increase in Ca²⁺ signal intensity (Fig. 6C,D), whereas the US-evoked Ca²⁺ signals remained unchanged (Fig. 6E). As the conditioning developed, the CS elicited an increasing trend in the intensity of Ca²⁺ signals, and the CS-evoked Ca²⁺ signals lasted through the delay period, reaching a peak following delivery of the US (Fig. 6C,D). These observations support that cued-aversion conditioning rapidly shaped the response of IPN neurons. Compared with WT mice, *KCTD8/12/16* KO mice responded to the CS and US with stronger Ca²⁺ signals during aversion conditioning sessions, suggesting a high sensitivity to aversive stimuli.

We tested whether KCTDs contributed to the expression and extinction of cued-aversion memory in the IPN. On the extinction days, the mice were introduced into a new test chamber with the same CS but omitting the US. The CS-evoked Ca²⁺ signal intensities were strong on extinction day 1 and then gradually decreased during the subsequent extinction days; the intensities were reduced significantly on extinction day 2 in WT mice, whereas on extinction day 3 in *KCTD8/12/16* KO mice (Fig. 6C, D, F). We monitored the locomotor activity of the mice. In the beginning trials, mice exhibited lower locomotion following the CS, indicating freezing levels during cued-aversive extinction sessions. After 10 trials of extinction, their locomotor activity during the CS period became higher than the initial level (Fig. 6G). These observations indicate the correlation of IPN neuronal activities with physiological freezing during extinction sessions. Thus, the fiber photometry recording suggests that *KCTD8/12/16* KO mice displayed enhanced neuronal responses to aversion-predicting cues in IPN neurons. Compared with wild-type mice, *KCTD8/12/16* triple KO mice showed hyperlocomotion (Fig. 6H), and exhibited lower locomotor activity during CS delivery in the cued-aversion conditioning and extinction sessions (Fig. 6G), which suggested changes in locomotor control and behavioral sensitivity to the formation and expression of cued-aversion memory.

KCTDs regulate baclofen-mediated fear extinction in the habenulo–interpeduncular pathway

There were some potential limitations for our data shown in Figure 6. First, we used the brief cue–footshock paradigm (2 s cue with 1 s delay before footshock), which differs from the standard fear conditioning paradigm that measures freezing behavior following long cues (20 s). Second, we recorded Ca²⁺ signals from the triple knock-out mice, whereas only *KCTD8* and *12* are important for axonal expression of GABA_B receptors in habenula cholinergic neurons. Third, knocking out *KCTD16* alone impairs the extinction of cued aversion memory (Cathomas et al., 2017). The hyperlocomotor phenotypes of the *KCTD8/12/16* triple knock-out mice might further confound the behavioral roles of KCTDs in the habenulo–interpeduncular pathway.

Considering that GABA_B activity facilitates fear extinction in the MHb–IPN pathway (Zhang et al., 2016) and mainly *KCTD8* and *KCTD12* are expressed in MHb neurons, we examined the behavioral phenotypes of *KCTD8/12* double knock-out mice using the standard fear conditioning and extinction paradigm (10 trials of 20 s cue with or without footshock for conditioning

and extinction, respectively; Fig. 7A). Baclofen (15 pmol) or ACSF control was infused into the IPN through an implanted cannula (Fig. 7B). Confirming that activating GABA_B receptors in the MHb–IPN pathway facilitates fear extinction (Zhang et al., 2016), baclofen infusion into the IPN significantly reduced the freezing time of WT mice in response to the cue during the extinction sessions on the 3 consecutive days (Fig. 7C,D). In contrast, baclofen infusions into the IPN of *KCTD8/12* double knock-out mice only mildly affected the freezing behavior during the extinction session and did not significantly change the overall freezing time (Fig. 7C,D). ACSF control infusions did not reveal a strong difference between WT mice and the mutant mice both during the condition sessions and the extinction sessions (Fig. 7C,D). In addition, the *KCTD8/12* double knock-out mice exhibited similar locomotor activity pattern at rest (Fig. 7E). These results thus suggested that KCTDs regulate the activity of GABA_B receptors in the habenulo–interpeduncular pathway to facilitate fear extinction rather than general locomotor activity.

Discussion

The richly expressed GABA_B receptors represent the principal inhibitory neurotransmitter receptors (Nishikawa et al., 1997; Couve et al., 2000; Chalifoux and Carter, 2011; Benke et al., 2012; Gassmann and Bettler, 2012; Pin and Bettler, 2016; Fritzius and Bettler, 2020). In the MHb–IPN pathway, GABA_B receptor is first reported to mediate presynaptic excitation via Ca_{v2.3} (Zhang et al., 2016). The exact molecular mechanism of this presynaptic excitation remain to be dissected. Several KCTD isoforms assemble with native GABA_B receptors (Schwenk et al., 2010, 2016), but their roles in mediating GABA_B receptors–mediated presynaptic expression and excitation remain unclear. By analyzing the effect of knocking out *KCTD8*, *12*, and *16* separately or in various combinations, in this study we find that *KCTD8* and *KCTD12* in habenula cholinergic neurons are important for facilitating the axonal expression and presynaptic excitation of GABA_B receptors. We further show that the KCTDs in the habenulo–interpeduncular pathway are important for regulating physiological responses during aversion memory formation and expression.

Our findings expand our understanding of functions of KCTD–GABA_B interactions in adult brains. KCTDs tightly assemble with GABA_B receptors to regulate the activation and desensitization of their effectors, including the G-protein-coupled inwardly rectifying potassium channels, the opening of which inhibits neurons. In the habenulo–interpeduncular pathway, GABA_B receptors mediate the presynaptic excitation via the R-type calcium channel Ca_{v2.3} (Zhang et al., 2016). A recent study reveals that *KCTD8* KO, *KCTD12b* KO, and *KCTD8/12b* double KO do not affect GABA_B receptors–mediated presynaptic excitation, whereas *KCTD8* and *KCTD12b* modulate Ca_{v2.3}-mediated release probability in the MHb–IPN pathway in a GABA_B receptors–independent manner (Bhandari et al., 2021). Here, we characterized the phenotypes of single, double, and triple knock-out of *KCTD8*, *12*, and *16*. Consistently, single knock-out of *KCTD8* does not affect the presynaptic excitation of GABA_B receptors. Rather, knocking out both *KCTD8* and *KCTD12* is required to produce a strong decrease in the potentiation effect of GABA_B receptors on neurotransmitter release and presynaptic Ca²⁺ entry. Overexpression experiments indicate that either isoform sufficiently rescues the knock-out phenotypes. Thus, our results, together with those by Bhandari et al. (2021), illustrate isoform-specific roles of KCTDs in synaptic transmission via interacting with GABA_B receptors in the brain.

←

the IPN of WT and *KCTD8/12/16* KO mice. **H**, Images from Allen Brain Atlas show the mRNA expression pattern of *KCTD8*, *12*, and *16* in the MHb and the IPN. Scale bars: 100 μm; **A–D**, top and bottom, 20 μm; **E, F**, 100 μm; and **H**, 400 μm.

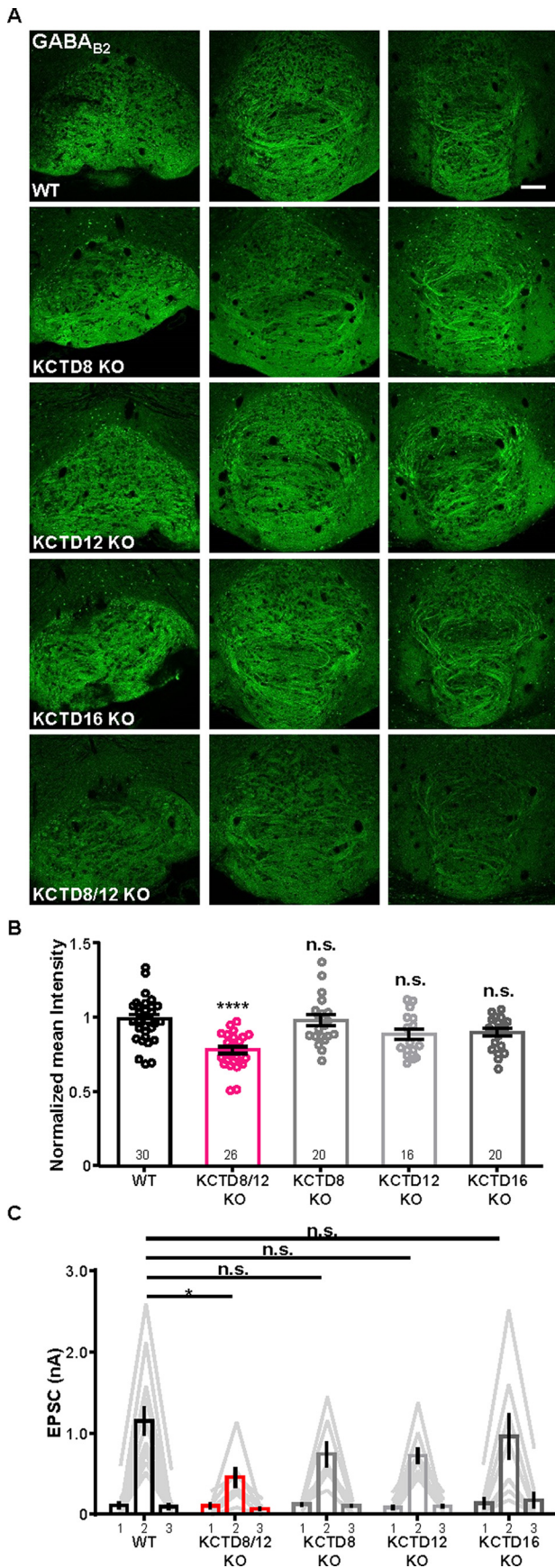


Figure 4. Knocking out both *KCTD8* and *KCTD12* reduces the axonal expression and presynaptic excitation of GABA_B receptors in habenula cholinergic neurons. **A**, Images show the immunoreactivity of GABA_{B2} receptors in the anterior, center, and posterior sections of the

Intriguingly, GABA_B receptors mediate excitation in the axonal terminals but inhibition in the somata/dendrites of habenula cholinergic neurons. We show that *KCTD8* and *KCTD12* together promote GABA_B expression and its excitatory effects in presynaptic terminals but are indispensable for GABA_B expression and its inhibitory effects in the somata. It has been reported that *KCTD12* promotes receptor expression at the cell surface by reducing GABA_B receptors internalization in COS-1 cells and cultured hippocampal neurons (Bartoi et al., 2010; Ivankova et al., 2013). Moreover, transfection of *KCTD12* into cultured hippocampal neurons increases the amount of GABA_B receptors primarily in axonal terminals but not in dendrites (Bartoi et al., 2010). This study reveals that both *KCTD8* and *KCTD12* contribute to GABA_B expression and signaling in the axonal terminals but not somata/dendrites, thus suggesting the presence of two distinct signaling pathways in MHb neurons, resulting in opposite function of GABA_B receptors in the axonal terminals and somata/dendrites. *KCTD8* and *KCTD12* are integral constituents of GABA_B receptors (Schwenk et al., 2010), which suggests that they may have a site-specific impact on the transport or surface stability of GABA_B receptors. Of note, knocking out both *KCTD8* and *KCTD12* reduces but does not abolish presynaptic excitation. This suggests the presence of a yet to be identified non-KCTD signaling component that switches the presynaptic GABA_B receptors in habenula cholinergic neurons from the common inhibition mode to the unique excitation mode.

The requirement of knocking out both *KCTD8* and *KCTD12* isoforms to reduce axonal GABA_B receptors expression indicates a compensatory effect of *KCTD8* and *KCTD12* in the MHb–IPN pathway. Bhandari et al. (2021) report that knocking out *KCTD12b* induces a compensatory increase of *KCTD8* at the active zone of the MHb terminals. It is thus possible that the genetic deficiency of a given isoform in the single *KCTD* KO mice might be compensated by other *KCTD* isoforms of similar functions. Indeed, the N-terminal regions of *KCTD8* and *KCTD12* are homologous to the BTB (BR-C, ttk and bab) domain which has adapted to several different modes of self-association (Stogios et al., 2005). This is further supported by our observation that over-expressing either *KCTD8* or *KCTD12* was sufficient to rescue the axonal expression and presynaptic excitation of GABA_B receptors in *KCTD8/12/16* KO mice. Therefore, although different *KCTD* isoforms may have distinct molecular features, the redundancy among various isoforms may require simultaneous knock-out to reveal their functional significance.

←

IPN of WT, *KCTD8* KO, *KCTD12* KO, *KCTD16* KO, and *KCTD8/12* double KO mice. Scale bars: 100 μm. **B**, Summary data show the mean intensity of GABA_{B2} immunoreactivity in the IPN of WT (1.00 ± 0.03, n = 30 slices from 6 mice), *KCTD8/12* KO (0.78 ± 0.02, n = 26 slices from 4 mice), *KCTD8* KO (0.98 ± 0.04, n = 20 slices from 3 mice), *KCTD12* KO (0.89 ± 0.04, n = 16 slices from 3 mice), and *KCTD16* KO (0.90 ± 0.03, n = 20 slices from 3 mice) mice. Data are normalized to the mean pixel intensity of WT mice within the same batch. n.s., Not significant. ****p < 0.0001; one-way ANOVA and Sidak's *post hoc* multiple comparisons test. **C**, Summary data show the peak amplitudes of evoked EPSCs before (1), during (2), and after (3) badofen treatment in the presence of a cocktail solution comprising picrotoxin, HMT, and Mec from IPN neurons of *Chat-ChR2* (I_{Basal} = 112.9 ± 44.7 pA; I_{Badofen} = 1152.6 ± 177.1 pA; I_{Wash} = 94.9 ± 43.9 pA; n = 13 cells from 5 mice), *KCTD8/12* KO::*Chat-ChR2* (I_{Basal} = 104.4 ± 37.4 pA; I_{Badofen} = 455.7 ± 128.3 pA; I_{Wash} = 66.2 ± 27.2 pA; n = 7 cells from 3 mice), *KCTD8* KO::*Chat-ChR2* (I_{Basal} = 124.9 ± 23.9 pA; I_{Badofen} = 738.8 ± 156.9 pA; I_{Wash} = 104.3 ± 25.9 pA; n = 7 cells from 3 mice), *KCTD12* KO::*Chat-ChR2* (I_{Basal} = 80.6 ± 30.2 pA; I_{Badofen} = 723.9 ± 101.7 pA; I_{Wash} = 98.9 ± 28.4 pA; n = 9 cells from 3 mice), and *KCTD16* KO::*Chat-ChR2* (I_{Basal} = 133.8 ± 74.3 pA; I_{Badofen} = 957.2 ± 284.8 pA; I_{Wash} = 175.1 ± 99.6 pA; n = 8 cells from 3 mice) mice. n.s., Not significant. p > 0.05; *p < 0.05; two-way ANOVA and Sidak's *post hoc* multiple comparisons test. Data are presented as means ± SEM (Table 1).

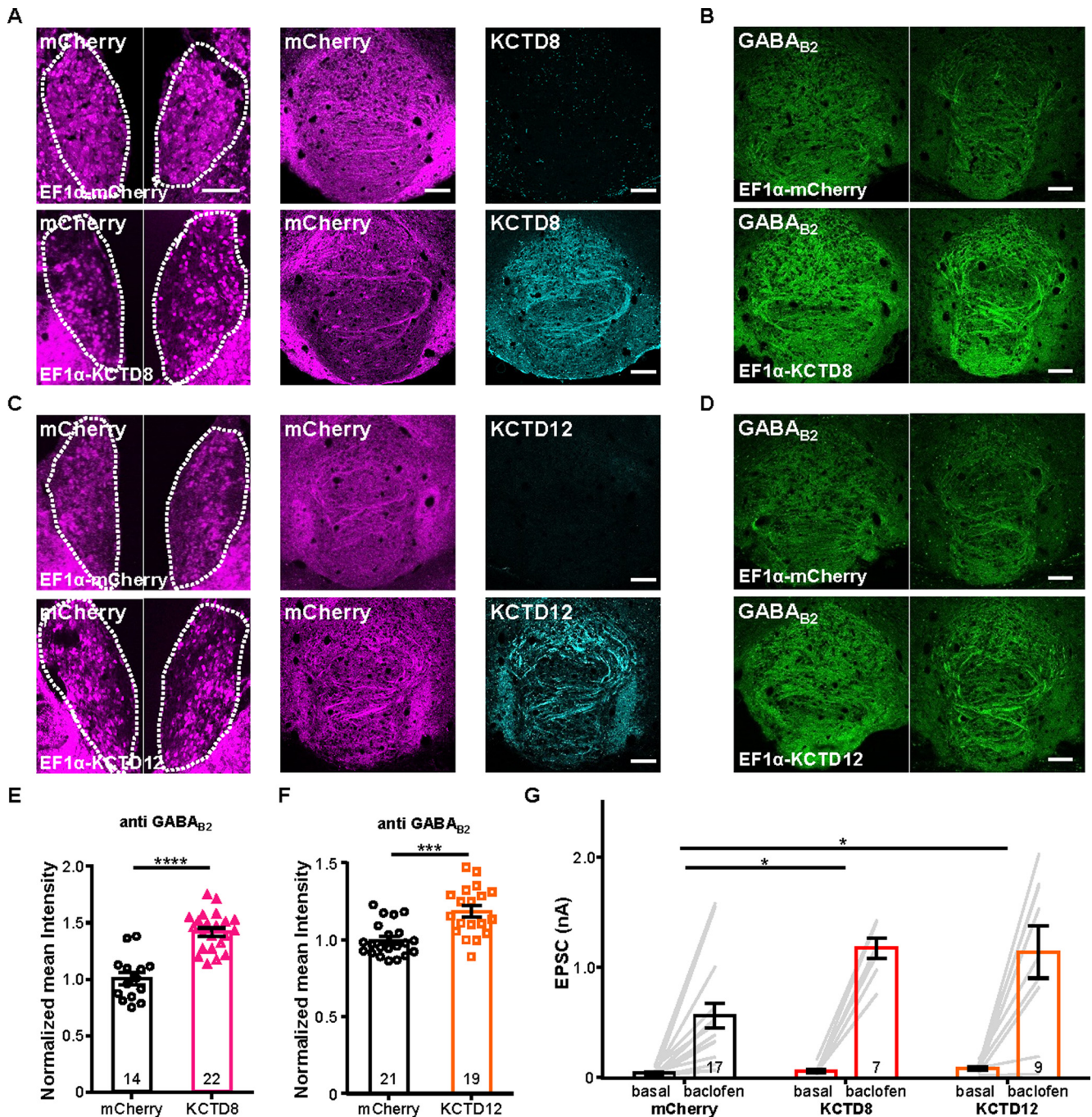


Figure 5. Overexpressing KCTD8 or KCTD12 in the MHb neurons of *KCTD8/12/16* KO mice rescues axonal GABA_B expression and presynaptic excitation. **A, B**, Example images show AAV transduction of AAV-mCherry (**A**, top) and KCTD8-P2A-mCherry (**A**, bottom) in MHb neurons and expression of mCherry in the axonal terminals within the IPN of *KCTD8/12/16* KO mice. AAV-KCTD8-P2A-mCherry but not AAV-mCherry in MHb neurons of *KCTD8/12/16* KO mice expressed KCTD8 (**A**) and increased the expression of GABA_{B2} in the axonal terminals within the IPN (**B**). **C, D**, The effect of overexpressing KCTD12 in habenula neurons on GABA_{B2} expression within the IPN of *KCTD8/12/16* KO mice. Same conventions as in **A, B, E, F**. Summary plots show the effect of overexpressing KCTD8 (mCherry: 1.00 ± 0.05, *n* = 14 slices; KCTD8: 1.41 ± 0.04, *n* = 22 slices; **E**) or KCTD12 (mCherry: 1.00 ± 0.02, *n* = 21 slices; KCTD12: 1.19 ± 0.04, *n* = 19 slices; **F**) on the mean intensity of GABA_{B2} immunoreactivity in the IPN. *****p* < 0.001, *****p* < 0.0001; unpaired *t* test (with Welch's correction). **G**, Summary data show the effect of overexpressing mCherry (*I*_{basal} = 45.6 ± 8.9 pA; *I*_{baclofen} = 567.3 ± 113.3 pA; *n* = 17 cells from 4 mice), KCTD8-P2A-mCherry (*I*_{basal} = 65.6 ± 17.0 pA; *I*_{baclofen} = 1179.5 ± 90.9 pA; *n* = 7 cells from 3 mice), and KCTD12-P2A-mCherry (*I*_{basal} = 87.2 ± 14.6 pA; *I*_{baclofen} = 1147.3 ± 239.4 pA; *n* = 9 cells from 5 mice) on basal and baclofen-potentiated, light-evoked EPSCs in the IPN neurons of *KCTD8/12/16* KO::*CHAT-ChR2* mice. **p* < 0.05; two-way ANOVA and Sidak's *post hoc* multiple comparisons test. Data are presented as means ± SEM (Table 1). Scale bars: 100 μm.

Our fiber photometry of behaving mice reveals the IPN neuronal response to aversion memory. Lesions of the habenulo-interpeduncular pathway impair the performance of the avoidance response and the consolidation and retrieval of aversive memories (Thompson, 1960; Zhao-Shea et al., 2015; McLaughlin et al., 2017; Vincenz et al., 2017; Khatami et al., 2018). Using

fiber photometry of Ca²⁺ signals in the IPN (Huang et al., 2019), we provide the first demonstration that cued-aversion conditioning can rapidly shape the response of IPN neurons, forming the physiological correlate of aversive memories. In *KCTD 8/12/16* triple knock-out mice, IPN neurons exhibit stronger Ca²⁺ signals to both the cue and the footshock. This observation seems

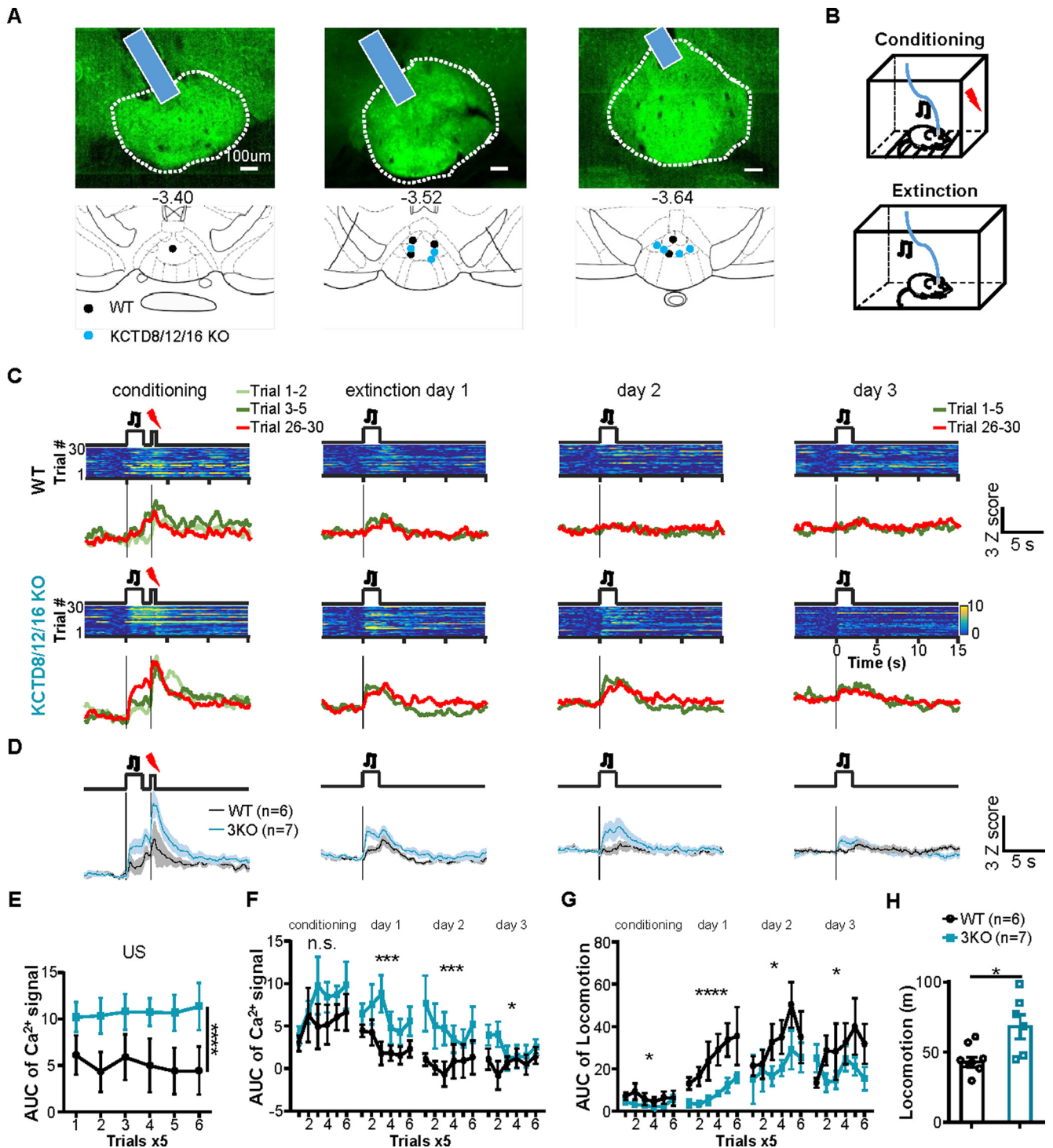


Figure 6. IPN neurons in *KCTD8/12/16* triple KO mice display enhanced Ca²⁺ signal responses to aversion-predicting cues. **A**, Expression of GCaMP6m and the placement of recording optical fiber (top), and schematic drawings of the optical fiber tips (bottom) in anterior and center and posterior sections of the IPN, corresponding approximately to bregma 3.4, 3.52, and 3.64 mm, respectively. Scale bars: 100 μm. **B**, Schematic diagram of the experimental design for the cued-aversion conditioning and extinction sessions. The conditioning sessions consisted of the deliveries of 30 discrete tone-footshock pairs, whereas the extinction sessions consisted of 30 tone deliveries. **C**, Trial-by-trial heatmaps and the peri-event plot of average Ca²⁺ signals illustrate example neuronal responses in cued-aversion conditioning sessions and extinction sessions in WT and *KCTD8/12/16* KO mice. The color code for the plots of Ca²⁺ signals, light green for trials 1–2, green for trials 3–5, and red for trials 26–30. **D**, Averaged Ca²⁺ signals of WT and *KCTD8/12/16* KO mice during the cued-aversion conditioning and extinction sessions. Shaded area indicates SEM. **E**, AUC of averaged Ca²⁺ signal responses (3–5 s) to footshocks in WT and *KCTD8/12/16* KO mice. Each data point represents the average of five consecutive trials, n.s., Not significant. *****p* < 0.0001; two-way ANOVA and Sidak's *post hoc* multiple comparisons test for the difference between the first data point and those of the following trials (n.s., no differences across all trials in WT or *KCTD8/12/16* KO mice), and for the difference of AUC between WT and *KCTD8/12/16* KO mice. **F**, AUC of averaged Ca²⁺ signal responses (0–3 s) to the auditory tones in WT and *KCTD8/12/16* KO mice. Each data point represents the average of five consecutive trials during cued-fear conditioning sessions and the extinction sessions on day 1–3, n.s., Not significant. **p* < 0.05, ****p* < 0.001; two-way ANOVA for the difference of AUC between WT and *KCTD8/12/16* KO mice. Two-way ANOVA for the difference of AUC between extinction day 1 and extinction day 2, 3 in WT mice (**p* < 0.05 between day 1 and day 2; ***p* < 0.01 between day 1 and day 3). Two-way ANOVA for the difference of AUC between extinction day 1 and extinction day 2, 3 in *KCTD8/12/16* KO mice (n.s., *p* > 0.05 between day 1 and day 2, ****p* < 0.001 between day 1 and day 3). **G**, AUC of averaged locomotion (0–3 s) during cued-fear conditioning

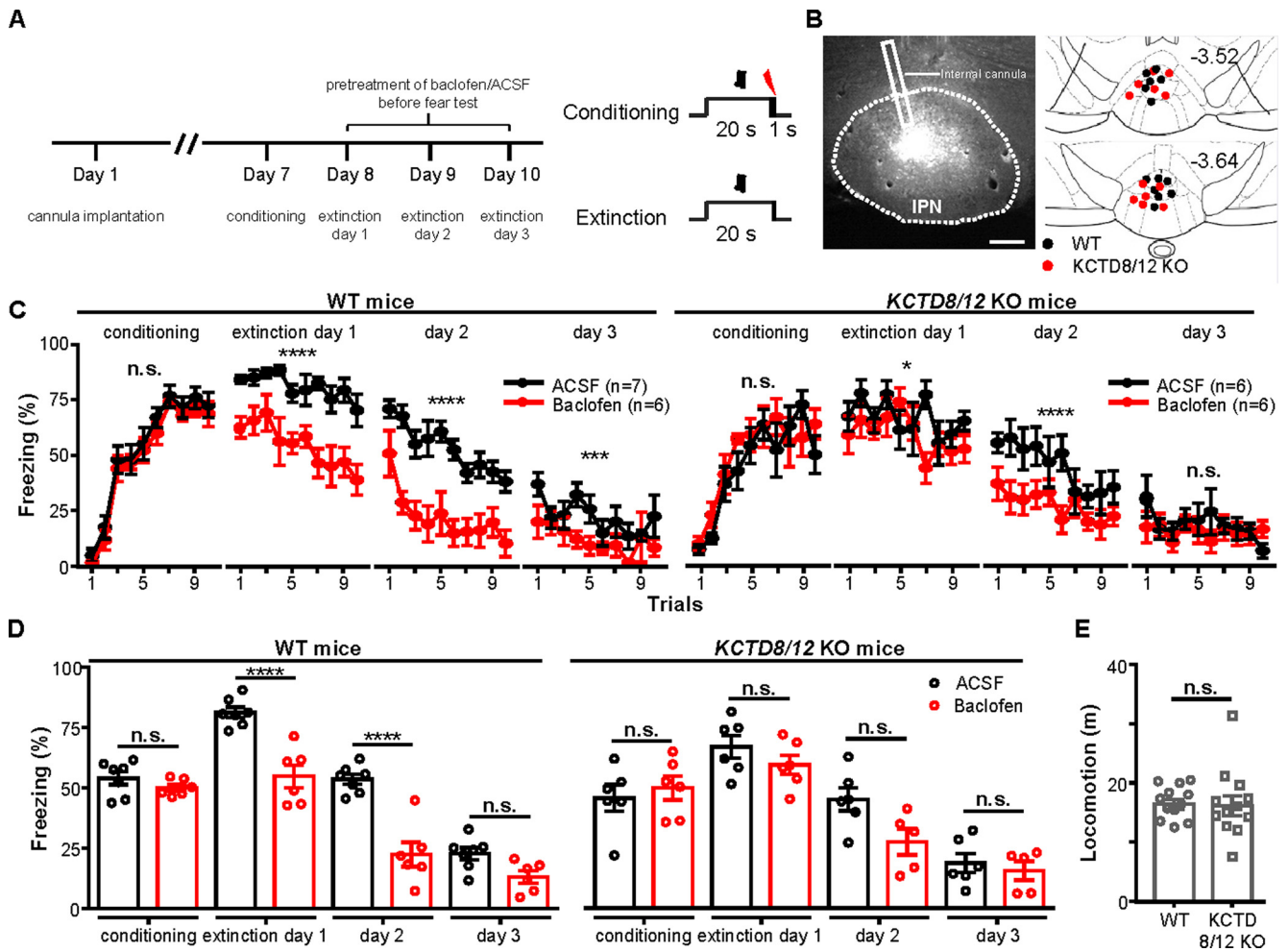


Figure 7. Knocking out *KCTD8/12* reduces the effect of baclofen on facilitating fear extinction. **A**, Experimental timeline (left) and the behavioral paradigms (right) for fear conditioning and fear extinction on the following 3 consecutive days. Mice were conditioned or tested for 10 trials in each session. **B**, Left, Image shows the cannula placement and the extent of the Texas Red dextran amines infusion following the behavioral tests. Scale bars: 200 μ m. Right, Images show the drug injection sites in anterior and posterior sections of the IPN, corresponding to 3.52 and 3.64 mm from bregma, respectively. **C**, Freezing responses across trials during cued-fear conditioning and extinction sessions of WT mice (left) and *KCTD8/12* KO mice (right), with the pretreatment of ACSF control (black) or baclofen (red; 15 pmol) during the extinction sessions. n.s., Not significant. * $p < 0.05$, *** $p < 0.001$, **** $p < 0.0001$; two-way ANOVA for the difference of AUC between ACSF and Baclofen. **D**, Total freezing durations of WT mice (left) and *KCTD8/12* KO mice (right) in each behavioral session. n.s., Not significant. **** $p < 0.0001$; one-way ANOVA for the difference of AUC between ACSF and Baclofen in the WT and *KCTD8/12* KO mice groups. **E**, Summary graphs depict the total locomotion in 3 min before fear condition without cue in the WT and *KCTD8/12* KO mice. n.s., Not significant. Unpaired *t* test (with Welch's correction). Data are presented as means \pm SEM (Table 1).

to be the opposite of what would be expected from the finding that the triple KO mice exhibit a decrease in neurotransmitter release from the habenula to the IPN. This might be reconciled by the fact that a majority of IPN neurons, including interneurons, are GABAergic (Zhao-Shea et al., 2013). The extensive GABAergic local circuits in the IPN might form a disinhibition mechanism that transforms a decrease in glutamatergic signal from the MHb to an enhancement in output from the IPN neurons of the triple knock-out mice. Future cell type-specific recordings and manipulations would help testing this scheme of microcircuitry in the IPN.

Our behavioral assays also indicate that KCTDs contribute to the regulation of aversion memory in the MHb–IPN pathway. In

accordance with impaired aversion extinction in GABA_B conditional knock-out in cholinergic neurons (Zhang et al., 2016), here we show that knocking out *KCTD8* and *KCTD12* reduces the effect of intra-IPN baclofen infusion on facilitating fear extinction. Unlike GABA_B knock-out mice (Zhang et al., 2016), the double knock-out mice do not exhibit a decrease in fear extinction in the control condition, possibly because the genetic deficiency of *KCTD8/12* reduces but does not abolish GABA_B presynaptic excitation. In addition, multiple GABA_B-associated KCTDs, such as *KCTD12* and *KCTD16*, are expressed in numerous brain areas and regulate aversive memory (Cathomas et al., 2015, 2017). Therefore, although our physiological and behavioral assays indicate an important role of KCTDs in regulating neurotransmission within the habenulo–interpeduncular pathway and its associated behavioral functions in cued-aversion memory, *KCTD8* and *KCTD12* outside the habenulo–interpeduncular pathway may also play a role in regulating aversive memory processes. Conditional knock-out of both *KCTD8* and *KCTD12* precisely in the habenula cholinergic neurons of adult mice would help

← sessions and the extinction sessions on day 1–3 in WT and *KCTD8/12/16* KO mice; * $p < 0.05$, **** $p < 0.001$. Two-way ANOVA for the difference of AUC between WT and *KCTD8/12/16* KO mice. **H**, Summary graphs depict the total locomotion in 10 min before fear condition without cue in the WT and *KCTD8/12* KO mice; * $p < 0.05$, unpaired *t* test (with Welch's correction). Data are presented as means \pm SEM (Table 1).

dissecting the precise behavioral functions of these two KCTD isoforms in the MHB.

Altogether, this study reveals that KCTD8/12 auxiliary subunits modulate the expression and function of GABA_B receptors in habenula cholinergic neurons, thereby affecting aversion memory processing in adult mice. Malfunctions in GABA_B receptors, KCTDs, and their interactions are involved in several neuropsychiatric disorders (Gassmann and Bettler, 2012; Cathomas et al., 2015, 2017). For example, *KCTD8* is associated with brain size and modulates the adverse effects of smoking during pregnancy on brain development (Paus et al., 2012). The *KCTD12* gene expression is associated with bipolar I disorder (Lee et al., 2011), depressive-like state (Sibille et al., 2009; Surget et al., 2009), and schizophrenia (Benes, 2010), whereas *KCTD16* is related to congenital partial epilepsy syndrome (Angelicheva et al., 2009). Given that the habenulo–interpeduncular pathway and the GABA_B signaling in this pathway regulates aversion-memory-associated behaviors in animals, our results suggest that regulating KCTD8/12-associated signaling in this neural pathway may have relevance to therapeutic interventions in related mental disorders.

References

- Ables JL, Görlich A, Antolin-Fontes B, Wang C, Lipford SM, Riad MH, Ren J, Hu F, Luo M, Kenny PJ, Heintz N, Ibañez-Tallon I (2017) Retrograde inhibition by a specific subset of interpeduncular alpha5 nicotinic neurons regulates nicotine preference. *Proc Natl Acad Sci U S A* 114:13012–13017.
- Agatsuma M, Aizawa H, Aoki T, Nakayama R, Takahoko M, Goto M, Sassa T, Amo R, Shiraki T, Kawakami K, Hosoya T, Higashijima S-i, Okamoto H (2010) The habenula is crucial for experience-dependent modification of fear responses in zebrafish. *Nat Neurosci* 13:1354–1356.
- Angelicheva D, Tournev I, Guergueltcheva V, Mihaylova V, Azmanov DN, Morar B, Radionova M, Smith SJ, Zlatareva D, Stevens JM, Kaneva R, Bojinova V, Carter K, Brown M, Jablensky A, Kalaydjieva L, Sander JW (2009) Partial epilepsy syndrome in a Gypsy family linked to 5q31.3-q32. *Epilepsia* 50:1679–1688.
- Bartoi T, Rigbolt KT, Du D, Köhr G, Blagoev B, Kornau HC (2010) GABA_B receptor constituents revealed by tandem affinity purification from transgenic mice. *J Biol Chem* 285:20625–20633.
- Benes FM (2010) Amygdalocortical circuitry in schizophrenia: from circuits to molecules. *Neuropsychopharmacology* 35:239–257.
- Benke D, Zemoura K, Maier PJ (2012) Modulation of cell surface GABA(B) receptors by desensitization, trafficking and regulated degradation. *World J Biol Chem* 3:61–72.
- Bhandari P, Vandael D, Fernández-Fernández D, Fritzius T, Kleindienst D, Önal C, Montanaro J, Gassmann M, Jonas P, Kulik A, Bettler B, Shigemoto R, Koppensteiner P (2021) GABA_B receptor auxiliary subunits modulate Cav2.3-mediated release from medial habenula terminals. *Elife* 10:e68274.
- Cathomas F, Stegen M, Sigrüst H, Schmid L, Seifritz E, Gassmann M, Bettler B, Pryce CR (2015) Altered emotionality and neuronal excitability in mice lacking KCTD12, an auxiliary subunit of GABA_B receptors associated with mood disorders. *Transl Psychiatry* 5:e510.
- Cathomas F, Sigrüst H, Schmid L, Seifritz E, Gassmann M, Bettler B, Pryce CR (2017) Behavioural endophenotypes in mice lacking the auxiliary GABA_B receptor subunit KCTD16. *Behav Brain Res* 317:393–400.
- Chalifoux JR, Carter AG (2011) GABA_B receptor modulation of synaptic function. *Curr Opin Neurobiol* 21:339–344.
- Couve A, Moss SJ, Pangalos MN (2000) GABA_B receptors: a new paradigm in G protein signaling. *Mol Cell Neurosci* 16:296–312.
- Frahm S, Slimak MA, Ferrarese L, Santos-Torres J, Antolin-Fontes B, Auer S, Filkin S, Pons S, Fontaine J-F, Tsetlin V, Maskos U, Ibañez-Tallon I (2011) Aversion to nicotine is regulated by the balanced activity of $\beta 4$ and $\alpha 5$ nicotinic receptor subunits in the medial habenula. *Neuron* 70:522–535.
- Frahm S, Antolin-Fontes B, Görlich A, Zander J-F, Ahnert-Hilger G, Ibañez-Tallon I (2015) An essential role of acetylcholine-glutamate synergy at habenular synapses in nicotine dependence. *Elife* 4:e11396.
- Fritzius T, Bettler B (2020) The organizing principle of GABA_B receptor complexes: physiological and pharmacological implications. *Basic Clin Pharmacol Toxicol* 126 Suppl 6:25–34.
- Fritzius T, Turecek R, Seddik R, Kobayashi H, Tiao J, Rem PD, Metz M, Kralikova M, Bouvier M, Gassmann M, Bettler B (2017) KCTD heterooligomers confer unique kinetic properties on hippocampal GABA_B receptor-induced K⁺ currents. *J Neurosci* 37:1162–1175.
- Gassmann M, Bettler B (2012) Regulation of neuronal GABA(B) receptor functions by subunit composition. *Nat Rev Neurosci* 13:380–394.
- Hu F, Ren J, Zhang JE, Zhong W, Luo M (2012) Natriuretic peptides block synaptic transmission by activating phosphodiesterase 2A and reducing presynaptic PKA activity. *Proc Natl Acad Sci U S A* 109:17681–17686.
- Huang L, Xi Y, Peng Y, Yang Y, Huang X, Fu Y, Tao Q, Xiao J, Yuan T, An K, Zhao H, Pu M, Xu F, Xue T, Luo M, So K-F, Ren C (2019) A visual circuit related to habenula underlies the antidepressive effects of light therapy. *Neuron* 102:128–142.e8.
- Isokawa M (1997) Membrane time constant as a tool to assess cell degeneration. *Brain Res Brain Res Protoc* 1:114–116.
- Ivanova K, Turecek R, Fritzius T, Seddik R, Prezeau L, Comps-Agrar L, Pin J-P, Fakler B, Besseyrias V, Gassmann M, Bettler B (2013) Up-regulation of GABA(B) receptor signaling by constitutive assembly with the K⁺ channel tetramerization domain-containing protein 12 (KCTD12). *J Biol Chem* 288:24848–24856.
- Khatami L, Khodaghali F, Motamedi F (2018) Reversible inactivation of interpeduncular nucleus impairs memory consolidation and retrieval but not learning in rats: a behavioral and molecular study. *Behav Brain Res* 342:79–88.
- Kim U (2009) Topographic commissural and descending projections of the habenula in the rat. *J Comp Neurol* 513:173–187.
- Kobayashi Y, Sano Y, Vannoni E, Goto H, Suzuki H, Oba A, Kawasaki H, Kanba S, Lipp H-P, Murphy NP, Wolfer DP, Itohara S (2013) Genetic dissection of medial habenula–interpeduncular nucleus pathway function in mice. *Front Behav Neurosci* 7:17.
- Lee MTM, Chen CH, Lee CS, Chen CC, Chong MY, Ouyang WC, Chiu NY, Chuo LJ, Chen CY, Tan HKL, Lane HY, Chang TJ, Lin CH, Jou SH, Hou YM, Feng J, Lai TJ, Tung CL, Chen TJ, Chang CJ, et al. (2011) Genome-wide association study of bipolar I disorder in the Han Chinese population. *Mol Psychiatry* 16:548–556.
- Lu L, Ren Y, Yu T, Liu Z, Wang S, Tan L, Zeng J, Feng Q, Lin R, Liu Y, Guo Q, Luo M (2020) Control of locomotor speed, arousal, and hippocampal theta rhythms by the nucleus incertus. *Nat Commun* 11:262.
- McLaughlin I, Dani JA, De Biasi M (2017) The medial habenula and interpeduncular nucleus circuitry is critical in addiction, anxiety, and mood regulation. *J Neurochem* 142 Suppl 2:130–143.
- Metz M, Gassmann M, Fakler B, Schaeren-Wiemers N, Bettler B (2011) Distribution of the auxiliary GABA_B receptor subunits KCTD8, 12, 12b, and 16 in the mouse brain. *J Comp Neurol* 519:1435–1454.
- Nishikawa M, Hirouchi M, Kuriyama K (1997) Functional coupling of Gi subtype with GABA_B receptor/adenylyl cyclase system: analysis using a reconstituted system with purified GTP-binding protein from bovine cerebral cortex. *Neurochem Int* 31:21–25.
- Paus T, Bernard M, Chakravarty MM, Davey Smith G, Gillis J, Lourdasamy A, Melka MG, Leonard G, Pavlidis P, Perron M, Pike GB, Richer L, Schumann G, Timpson N, Toro R, Veillette S, Pausova Z (2012) KCTD8 gene and brain growth in adverse intrauterine environment: a genome-wide association study. *Cereb Cortex* 22:2634–2642.
- Pin JP, Bettler B (2016) Organization and functions of mGlu and GABA_B receptor complexes. *Nature* 540:60–68.
- Qin C, Luo M (2009) Neurochemical phenotypes of the afferent and efferent projections of the mouse medial habenula. *Neuroscience* 161:827–837.
- Quina LA, Wang S, Ng L, Turner EE (2009) Brn3a and Nurr1 mediate a gene regulatory pathway for habenula development. *J Neurosci* 29:14309–14322.
- Rajalu M, Fritzius T, Adelfinger L, Jacquier V, Besseyrias V, Gassmann M, Bettler B (2015) Pharmacological characterization of GABA_B receptor subtypes assembled with auxiliary KCTD subunits. *Neuropharmacology* 88:145–154.
- Ren J, Qin C, Hu F, Tan J, Qiu L, Zhao S, Feng G, Luo M (2011) Habenula “cholinergic” neurons co-release glutamate and acetylcholine and activate

- postsynaptic neurons via distinct transmission modes. *Neuron* 69:445–452.
- Schwenk J, Metz M, Zolles G, Turecek R, Fritzius T, Bildl W, Tarusawa E, Kulik A, Unger A, Ivankova K, Seddik R, Tiao JY, Rajalu M, Trojanova J, Rohde V, Gassmann M, Schulte U, Fakler B, Bettler B (2010) Native GABA(B) receptors are heteromultimers with a family of auxiliary subunits. *Nature* 465:231–235.
- Schwenk J, Pérez-Garci E, Schneider A, Kollwe A, Gauthier-Kemper A, Fritzius T, Raveh A, Dinamarca MC, Hanuschkin A, Bildl W, Klingauf J, Gassmann M, Schulte U, Bettler B, Fakler B (2016) Modular composition and dynamics of native GABA(B) receptors identified by high-resolution proteomics. *Nat Neurosci* 19:233–242.
- Seddik R, Jungblut SP, Silander OK, Rajalu M, Fritzius T, Besseyrias V, Jacquier V, Fakler B, Gassmann M, Bettler B (2012) Opposite effects of KCTD subunit domains on GABA(B) receptor-mediated desensitization. *J Biol Chem* 287:39869–39877.
- Sibille E, Wang Y, Joeyen-Waldorf J, Gaiteri C, Surget A, Oh S, Belzung C, Tseng GC, Lewis DA (2009) A molecular signature of depression in the amygdala. *Am J Psychiatry* 166:1011–1024.
- Soria-Gómez E, Busquets-García A, Hu F, Mehdi A, Cannich A, Roux L, Louit I, Alonso L, Wiesner T, Georges F, Verrier D, Vincent P, Ferreira G, Luo M, Marsicano G (2015) Habenular CB1 receptors control the expression of aversive memories. *Neuron* 88:306–313.
- Stogios PJ, Downs GS, Jauhal JJ, Nandra SK, Privé GG (2005) Sequence and structural analysis of BTB domain proteins. *Genome Biol* 6:R82.
- Surget A, Wang Y, Leman S, Ibarguen-Vargas Y, Edgar N, Griebel G, Belzung C, Sibille E (2009) Corticolimbic transcriptome changes are state-dependent and region-specific in a rodent model of depression and of antidepressant reversal. *Neuropsychopharmacology* 34:1363–1380.
- Teng X, Aouacheria A, Lionnard L, Metz KA, Soane L, Kamiya A, Hardwick JM (2019) KCTD: a new gene family involved in neurodevelopmental and neuropsychiatric disorders. *CNS Neurosci Ther* 25:887–902.
- Thompson R (1960) Interpeduncular nucleus and avoidance conditioning in the rat. *Science* 132:1551–1553.
- Turecek R, Schwenk J, Fritzius T, Ivankova K, Zolles G, Adelfinger L, Jacquier V, Besseyrias V, Gassmann M, Schulte U, Fakler B, Bettler B (2014) Auxiliary GABA(B) receptor subunits uncouple G protein β γ subunits from effector channels to induce desensitization. *Neuron* 82:1032–1044.
- Vincenz D, Wernecke KEA, Fendt M, Goldschmidt J (2017) Habenula and interpeduncular nucleus differentially modulate predator odor-induced innate fear behavior in rats. *Behav Brain Res* 332:164–171.
- Yamaguchi T, Danjo T, Pastan I, Hikida T, Nakanishi S (2013) Distinct roles of segregated transmission of the septo-habenular pathway in anxiety and fear. *Neuron* 78:537–544.
- Zhang BB, Yao YY, Zhang HF, Kawakami K, Du JL (2017) Left habenula mediates light-preference behavior in zebrafish via an asymmetrical visual pathway. *Neuron* 93:914–928.e4.
- Zhang J, Tan L, Ren Y, Liang J, Lin R, Feng Q, Zhou J, Hu F, Ren J, Wei C, Yu T, Zhuang Y, Bettler B, Wang F, Luo M (2016) Presynaptic excitation via GABA(B) receptors in habenula cholinergic neurons regulates fear memory expression. *Cell* 166:716–728.
- Zhao-Shea R, Liu L, Pang X, Gardner PD, Tapper AR (2013) Activation of GABAergic neurons in the interpeduncular nucleus triggers physical nicotine withdrawal symptoms. *Curr Biol* 23:2327–2335.
- Zhao-Shea R, DeGroot SR, Liu L, Vallaster M, Pang X, Su Q, Gao G, Rando OJ, Martin GE, George O, Gardner PD, Tapper AR (2015) Increased CRF signalling in a ventral tegmental area-interpeduncular nucleus-medial habenula circuit induces anxiety during nicotine withdrawal. *Nat Commun* 6:6770.
- Zheng S, Abreu N, Levitz J, Kruse AC (2019) Structural basis for KCTD-mediated rapid desensitization of GABA(B) signalling. *Nature* 567:127–131.
- Zuo H, Glaaser I, Zhao Y, Kurinov I, Mosyak L, Wang H, Liu J, Park J, Frangaj A, Sturchler E, Zhou M, McDonald P, Geng Y, Slesinger PA, Fan QR (2019) Structural basis for auxiliary subunit KCTD16 regulation of the GABA(B) receptor. *Proc Natl Acad Sci U S A* 116:8370–8379.